University of Salerno
Department of Chemistry and Biology

Ph.D Course in Chemistry
(XXX Cycle)

Integrated techniques for remediation of dense chlorinated solvents polluted sites

Supervisor
Prof. Stefano Castiglione

Ph.D Student
Adriano Intiso

Co-Supervisor
Dr. Federico Rossi

Scientific referee
Prof. Antonio Proto

External referee
Prof. José Jorge Delgado García
(Universidad de Guanajuato)

Prof. Antonio Eduardo Palomares
(Universidad Politécnica de Valencia)

Ph.D Course Coordinator
Prof. Gaetano Guerra

Academic year 2016-2017

"L'uso corretto della scienza non sta nel dominare la natura, ma nel vivere in accordo con essa"

Enzo Tiezzi
(Tempi storici, tempi biologici)

Acknowledgements

Ed eccomi qui alla fine di questi tre anni a dover tirare le somme e riassumere tanta passione e fatica messi in questo progetto.

Il primo ringraziamento va al professore Rossi per questi quattro anni di duro lavoro e di sfide affrontate insieme. Dico quattro perché tutto è nato quasi per gioco durante la mia tesi magistrale, partendo da un episodio di contaminazione da tricloroetilene nel vicino comune di Solofra. Non avrei mai potuto mai immaginare di ritrovarmi qui dopo quattro anni a scrivere queste righe. Grazie davvero per i consigli (a volte anche schietti e diretti), gli sproni e gli incoraggiamenti che mi hanno permesso di crescere sia sotto l'aspetto umano che quello scientifico.

Il secondo ringraziamento va al professore Proto per la sua costante presenza in tutto il mio percorso accademico. E' stato lui ad instradarmi sulla chimica dell'ambiente e questo non potrò mai dimenticarlo. Un caloroso ringraziamento va anche al professore Castiglione e al suo gruppo di ricerca (Angela e Francesco); grazie all'opportunità concessami hanno reso il mio dottorato un percorso completo e interdisciplinare. La costante e proficua collaborazione con il mondo della biologia mi ha permesso di capire il vero senso della parola "interdisciplinarità".

Un grazie a tutti i miei colleghi del lab 8 (Maria, Ylenia, Ilaria, Emanuele e Marianna), in particolar modo a Raffaele, Milo e Concetta per le risate, le gioie, le fatiche e anche le incomprensioni che ci sono state in questi cinque anni. Tutto ciò ha contribuito allo sviluppo e alla formazione del mio essere.

Un ringraziamento speciale va all'Instituto de Tecnología Química dell'Università Politecnica di Valencia. Mi preme sinceramente ringraziare Edu e Ximo per l'opportunità concessami di spendere sei mesi del mio dottorato in questo fantastico istituto e di aver avuto l'onore di poter collaborare con loro. A tal proposito ringrazio alcuni dei colleghi e amici conosciuti che hanno reso questa esperienza una fantastica avventura, in particolar modo Jesus, Maria, Edi, Lidia, Marta Jose, Aitor, Rocio, Helena, le due Cris, Xelo, Belen, Teresa, Vicente, Andrea.

Grazie anche a Domb, mio unico e sincero amico da una vita; grazie anche per essere stato di supporto alla mia terribile sintassi inglese.

Arriviamo verso la fine…. Ma come si suol dire gli ultimi saranno i primi….

Un grandissimo grazie alla mia famiglia per avermi spronato ogni giorno a superare sempre i miei limiti. La mela non cade lontano dall'albero; se oggi nel bene e nel male sono Adriano

Intiso è anche merito loro. A questo punto è il momento di ringraziare la mia fidanzata Anna. Nel caos entropico della mia vita lei è l'unica che viola la seconda legge della termodinamica mettendo spesso ordine e sicurezza laddove io non riesco. I miei successi sono anche i suoi successi.
Credo davvero di aver terminato… This is it!!! =)

List of Publications

- Budroni M.A., Carballido-Landeira J., Intiso A., De Wit A., Rossi F. Interfacial hydrodynamic instabilities driven by cross-diffusion in reverse microemulsions, *Chaos Interdisc. J. Nonlinear Sci.* 25 (6), (2015), 064502

- Rossi F., Cucciniello R., Intiso A., Proto A., Motta O. Marchettini N. Determination of the trichloroethylene diffusion coefficient in water, *AIChE Journal* 61(10), (2015), 3511–3515

- Budroni M.A., Carballido-Landeira J., Intiso A., Lemaigre L., De Wit, A., Rossi F. From Microscopic Compartmentalization to Hydrodynamic Patterns New Pathways for Information Transport, *Communications in Computer and Information Science*, (2016), 171-183

- Moccia E., Intiso A., Cicatelli A., Proto A., Guarino F., Iannece P., Castiglione S., Rossi F. Use of Zea mays L. in phytoremediation of Trichloroethylene, *Environmental Science and Pollution Research*, 24 (12), (2017), 11053-11060

- Cucciniello R., Intiso A., Castiglione S., Genga A., Proto A. and Rossi F. Total oxidation of trichloroethylene over mayenite ($Ca_{12}Al_{14}O_{33}$) catalyst, *Applied Catalysis B: Environmental*, 204, (2017), 167-172

- Intiso A., Cucciniello R., Castiglione S., Proto A. and Rossi F. Environmental Application of Extra-Framework Oxygen Anions in the Nano-Cages of Mayenite., *Advances in Bionanomaterials*, (2017), 131-139

- Intiso A., Miele Y., Marchettini N., Proto A., Sánchez-Domínguez M., Rossi F. Enhanced solubility of trichloroethylene (TCE) by a polyoxyethylene alcohol as green surfactant. Submitted, 2017

- Intiso A., Martinez-Triguero J., Cucciniello R., Palomares Gimeno A.E. and Rossi F. Influence of the synthesis method on the catalytic activity of mayenite for the oxidation of gas-phase trichloroethylene. Submitted, 2017

Congress presentations

- Rossi F., Intiso A., Cucciniello R., Motta O., Marchettini N., Proto A. A new technique for the determination of trichloroethylene diffusion matrix in water, *Proceedings of XXV Congresso della Società Chimica Italiana*, 7-12 September 2014, Rende, Italy

- Rossi F., Cucciniello R., Intiso A., Motta A., Marchettini N., Proto A. Determination of Trichloroethylene diffusion matrix in water and micellar solutions, *Proceedings of XV Congresso Nazionale Chimica dell'Ambiente e dei beni culturali*, 14-18 June 2015, Bergamo, Italy

- Intiso A., Moccia E., Proto A., Iannece P., Rossi F., Cicatelli A., Castiglione S. Strategie di fitorisanamento di siti contaminati da solventi clorurati mediante l'impiego della Zea Mays L., *Proceedings of XV Congresso Nazionale Chimica dell'Ambiente e dei beni culturali*, 14-18 June 2015, Bergamo, Italy

- Carballido-Landeira J., Budroni M.A., Intiso A., De Wit A., Rossi F. Cross diffusion driven buoyant instabilities, *Proceedings of Bifurcations and instabilities in Fluid Dynamics, ESPCI* 15-17 July 2015, Paris, France

- Budroni M.A., Carballido-Landeira J., Intiso A., De Wit A., Rossi F. From compartmentalized systems to hydrodynamic instabilities: New pathways for information transport diffusion driven buoyant instabilities, *Proceedings of WIVACE 2015*, 23-25 September 2015, Bari, Italy

- Intiso A., Moccia E., Cicatelli A., Castiglione S., Proto A. Rossi F. Phytoremediation of contaminated sites by Trichloroethylene using Zea Mays L., *Proceedings of International Conference on Chemistry and the Environment 2015*, 20-24 September 2015, Leipzig, Germany

- Intiso A., Cucciniello R., Pironti C., Motta O., Proto A., Rossi F. Transport properties of Trichloroethylene in water and micellar solutions, *Workshop Chimica, Ambiente e Territorio*, 30 September 2015, Caserta, Italy

- Pironti C., Zarrella I., Proto A., Rossi F., Intiso A., Cucciniello R., Motta O. Applicazioni di nuovi metodi analitici per la determinazione del rapporto degli isotopi stabili del carbonio in ambito ambientale ed alimentare, *Workshop Chimica, Ambiente e Territorio*, 30 September 2015, Caserta, Italy

- Intiso A., Cucciniello R., Castiglione S., Proto A., Rossi F. Impiego della Mayenite nella catalisi ossidativa del Tricloroetilene, *Proceedings of XVI Congresso Nazionale Chimica dell'Ambiente e dei beni culturali*, 26-29 June 2016, Lecce, Italy

- Intiso A., Cucciniello R., Castiglione S., Proto A., Rossi F. A new green catalyst for the total oxidation of Trichloroethylene, *Proceedings of 6° Euchems Chemistry Congress*, 11 – 15 September 2016, Sevilla, Spain

- Intiso A., Cucciniello R., Castiglione S., Proto A., Rossi F. Environmental Application of Extra-Framework Oxygen Anions in the Nano-cages of Mayenite, *Proceedings of 11° Italian Workshop on Artificial Life and Evolutionary Computation/ 2° Workshop on Bionanomaterials,* 4-7 October 2016, Salerno, Italy

- Intiso A., Castiglione S., Dominguez M.S., Rossi Solubilization capabilities of a green surfactant towards DNAPLs, *Proceedings of Merck Young Chemists*

Symposium, 25-27 October 2016 , Rimini, Italy

- Intiso A., Gracia Soguero J.A., Rossi F., Palomares Gimeno A.E., Martínez-Triguero J. Beta zeolite and mayenite as catalysts for the trichloroethylene oxidation, *Proceedings of SECAT 2017 (Meeting of the Spanish Catalysis Society)*, 26-28 June 2017, Oviedo, Spain

- Intiso A., Cucciniello R., Castiglione S., Martínez-Triguero J. Proto A., Palomares Gimeno A.E., Rossi F. Catalytic oxidation of trichloroethylene over mayenite: Influence of the preparation method on the catalytic activity, *Proceedings of XXVI Congresso della Società Chimica Italiana*, 10-14 September 2017, Salerno, Italy

- Gracia Soguero J.A., Intiso A., Martínez-Triguero J., Rossi F., Palomares Gimeno A.E. Cobalt beta zeolite catalyst for the trichloroethylene oxidation, *Proceedings of XXVI Congresso della Società Chimica Italiana*, 10-14 September 2017, Salerno, Italy

- Intiso A., Martínez-Triguero J., Cucciniello R., Palomares Gimeno A.E., Rossi F. Improved mayenite features using PMMA as a soft template agent and its application in Cl-VOCs oxidation, *Proceedings of Merck Young Chemists Symposium,* 13-15 November 2017 , Milano marittima, Italy

Co-Supervisor of Thesis

- A.A. 2015-2016, Fabio Caldiero, Bachelor Thesis on Environmental Science, "Metodi per la distruzione catalitica del Tricloroetilene in fase gassosa"

- A.A. 2015-2016, Pietro Competiello, Bachelor Thesis on Environmental Science, "Studio del processo di solubilizzazione del tricloroetilene mediante l'impiego di un green-surfactant"

- A.A. 2016-2017, Michele Napoli, Bachelor Thesis on Environmental Science, “Distruzione catalitica del tricloroetilene mediante materiali a basso impatto ambientale”

- A.A. 2016-2017, Jesus A. Gracia Soguero, Master Thesis on Sustainable Chemistry, “Oxidación catalítica de tricloroetileno (TCE) en emisiones gaseosas con cobre/cobalto soportado sobre zeolita Beta”

- A.A. 2016/2017, Federica Borzelli, Bachelor Thesis on Chemistry, “Determinazione dei coefficienti di diffusione di bromato di sodio, bromuro di potassio e acido malonico in soluzioni binarie acquose tramite il metodo di dispersione di Taylor ”

Table of contents

Index of figures

Index of tables

Abstract

Trichloroethylene (TCE) is a halogenated aliphatic organic compound frequently detected as pollutant in soils and ground water.

A multidisciplinary approach is often required to remediate TCE polluted sites and this PhD thesis faces this problem blending together three main topics, namely surfactant co-solvent flushing, phytoremediation and catalytic oxidation, to develop an effective remediation strategy.

First of all we studied the diffusion mechanism of TCE in water to improve the models employed to describe the fate of the pollutant in the groundwater. In particular, we measured for the first time, the diffusion coefficient of TCE in water ($8.16 \pm 0.06 \times 10^{-6}$ cm^2s^{-1}). Moreover, we tested a commercially available, low-impact and biodegradable green surfactant, namely Synperonic 91/5 (Syn 91/5), to enhance the aqueous solubility of trichloroethylene. The results showed that Syn 91/5 allowed to increase up to 15 times the TCE aqueous solubility. The aim of this part of the work is to improve surfactant co-solvent flushing technology using eco-compatible and low cost surfactants.

In a later stage, we investigated the use of the plant *Zea mays* L. for the removal of high TCE concentrations from a growing medium, intended to be a laboratory model for soils

and water phytoremediation. In previous works, Mays plants were successfully used for the phytoextraction of heavy metals contaminated sites. The idea was to exploit the phytoremediation capability of *Z. mays* for the remediation of TCE polluted sites. The results showed that in 9 days of exposition, the plant was able to metabolize TCE with an efficiency ranging from 15 to 20 %, depending on the total amount of the pollutant added in the system.

Finally, we investigated a new green material to be used as catalyst for the total oxidation of TCE. Mayenite (C12A7) is a low cost material recently employed as active catalyst for several reactions. In this project we demonstrated that mayenite is able to oxidize TCE with better performances with respect to zeolites and other traditional catalysts. In particular, mayenite promoted the total oxidation of TCE in the temperature range 250-500° C, and the pollutant was converted in less harmful products such as CO_2, CO and HCl.

Overview

In 1984 Enzo Tiezzi wrote his book “Tempi storici, tempi biologici” (The End of Time)[1], in which he discussed the consequences of human industrialization on the health of the planet Earth. Moreover he indicated some guidelines to mitigate the problem of pollution and how humans could move towards a more eco-sustainable world.

After 30 years, the same themes discussed in this book are still up-to-date. Nowadays, the integrity of almost all environmental compartments is seriously threatened by contaminants and pollutants, which represent a danger for the present and the future generations.

Dense non-aqueous phase liquids (DNAPLs) are a family of organic compounds, often employed as degreasing agents in dry cleaning applications.

Trichloroethylene (TCE) used to be one of the most used organic solvent belonging to this family. DNAPLs show high chemical stability and persistence into the environment, due to their physical and chemical properties, and their remediation is a scientific and technological challenge. In the last years, in fact, a consistent part of the scientific research focused on finding new green solutions for the clean-up of DNAPLs polluted sites. In order to obtain an efficient remediation strategy, a multidisciplinary approach is often required.

This PhD thesis represents the attempt to answer to this open question through an interdisciplinary work. In particular three remediation techniques were investigated with the aim to improve the technology in terms of environmental sustainability and costs.

Initially, we measured for the first time the diffusion coefficient of TCE in water. A precise measure of this parameter is important for the improvement of the advection-diffusion (dispersion) models, generally employed to predict the fate of TCE in the environment before and during the remediation strategy.

In a later stage, we tested the potential use of an ethoxylated biodegradable alcohol (Synperonic 91/5) in the surfactant co-solvent flushing technology for TCE remediation. In particular we evaluated the improvement of TCE aqueous solubility by using this eco-friendly surfactant.

Another topic studied during this project was the employment of plants for the clean-up of TCE polluted sites. In this context, we successfully used mays plants for the remediation of artificial soil contaminated by TCE.

The last part of my PhD project was spent in the development of ceramic materials with low environmental impact as catalysts for the total oxidation of gaseous TCE. As a first step, we designed and realized a homemade apparatus to

perform the catalytic tests. Later, we assessed the catalytic activity, in terms of conversion rate and selectivity, of the material (mayenite) for the TCE oxidation reaction, obtaining good results.

Further investigations about the catalytic oxidation of TCE were performed during an Erasmus traineeship project of six months at the Institute of Chemical Technology-Polytechnic University of Valencia, where we had the opportunity to work in the group of Prof. Palomares and Dr. Martinez-Triguero.

An important aspect I would like to point out, concerns the collaborations developed during this period. The results obtained during my PhD were possible only thanks to the strong interaction with other groups, in particular with the group of Prof. Sanchez-Dominguez at CIMAV (Centro de Investigación en Materiales Avanzados of Monterrey, Mexico) and with the group of Prof. Palomares at the Institute of Chemical Technology-Polytechnic University of Valencia (ITQ-UPV, Spain).

"Collaboration is the essence of science"

Reference

(1) "Tempi storici, Tempi biologici" Enzo Tiezzi, GARZANTI, Milano1984.
English Edition:
The End of Time (The Sustainable World) Enzo Tiezzi, WITPRESS, Southampton (UK) 2002.

Synopsis

Chapter 1 briefly describes the environmental problems related with DNAPLs, with a focus on TCE, in particular: on its physico-chemical properties, on its effects on the human health, on the legislation regulating its presence in the environment and on the current remediation technologies.

Chapter 2 is about the fate and the transport mechanism of DNAPLs in the groundwater. In this context, we will present a method that allowed, for the first time, to measure the diffusion coefficient of TCE in water solutions.

In chapter 3 we will discuss about two remediation techniques investigated during this project. First, we will show the results on the capability of the green-surfactant Synperonic 91/5 (Syn 91/5) to improve the aqueous solubility of TCE.

Secondly, we will present the results about the use of phytoremediation as an alternative green technology for the removal of DNAPLs from polluted soils and waters. In particular, the employment of *Zea mays* L. for the effective remediation of TCE from a laboratory artificial contaminated soil will be discussed.

Chapter 4 will be about the use of eco-friendly ceramic materials as catalysts for the total oxidation of TCE. In particular, we will show that mayenite ($Ca_{12}Al_{14}O_{33}$) and Fe_2O_3-mayenite are able to oxidize TCE with comparable

performances of more expensive materials traditionally employed for this task. Moreover we will spend few words about the most important results obtained during the period as visiting student at ITQ-UPV.

Finally, in the conclusions, we will summarize and discuss the results obtained and the future perspectives of this project.

CHAPTER I: Introduction

1.1 DNAPLs and trichloroethylene: a persistent problem of the environment

Dense non-aqueous phase liquids (DNAPLs) are a class of organic compounds that include chlorinated volatile organic compounds (Cl-VOCs) and polycyclic aromatic hydrocarbons (PAHs)[1]. The physical and chemical properties of DNAPLs, especially the low solubility in water, the high density and the high affinity for organic compounds, are the cause of their persistence into the environment[2,3]. In the last years, several remediation strategies have been developed for the removal of DNAPLs from ground and surface waters, including: air stripping, adsorption processes, bioremediation, pump and treat and surfactant enhanced dissolution[4-7]. The latter will be discussed in details in section 1.4.

DNAPLs have been widely used as solvents for waxes, resins, fats, rubbers, oils and paints, and have also been extensively employed for dry cleaning and metal degreasing since 1920s[8].

Trichloroethylene (TCE) is a chlorinated solvent that belongs to the class of DNAPLs pollutants[9]. It is a colorless non-flammable liquid, hardly soluble in water with a sweet smell. TCE is commonly used in adhesive solvents, paints, and varnishes, and as metal degreaser for industrial application.

TCE can be introduced into the environment *via* water discharges during production processes, as vapor during degreasing operations or by accidental spills or intentional dumping (Figure 1.1) [10,11].

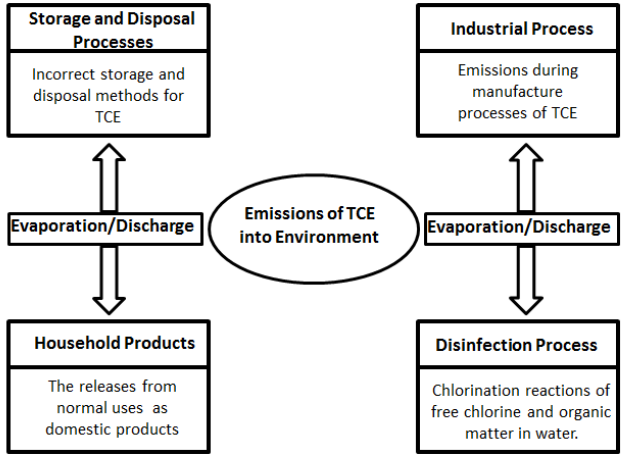

Figure 1.1 Principal emission sources of TCE into the environment

In addition it is chemically stable and generally inert toward biological degradation in aquifers, with half-lives measured in years, thus being a long-term source of contamination due to limited solubility and low mass-transfer rates.

1.2 Human health effects of trichloroethylene

Human exposure to TCE may happen *via* different routes. Because of the TCE high volatility, inhalation is its first way to enter in the human body. Ingestion and dermal absorption

are two other important routes of human exposure to TCE. Figure 1.2 summarizes the different ways of human exposure to TCE[12].

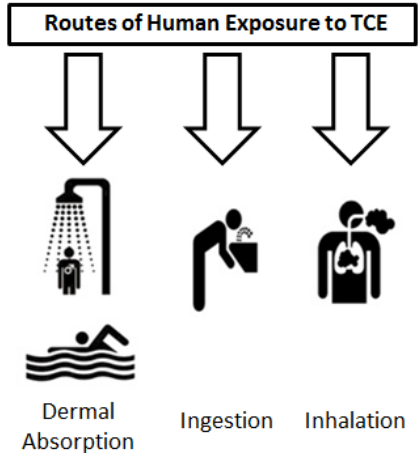

Figure 1.2 Primary routes of people exposure to TCE

The health effects of trichloroethylene depend on the amount of pollutant assumed and on the length of the exposure to the contaminant.

It has been reported that the exposition to TCE adversely affect the central nervous system, the immune system, the liver and the reproductive system[13].

TCE is metabolized by humans through different metabolic pathways, being the most important the oxidation and the glutathione GSH-conjugation, with the subsequent production of several toxicologically active compounds. Concerning the oxidation, the oxidative metabolites observed are

trichloroacetic acid (TCA), dichloroacetic acid (DCA) and chloral hydrate, where for the GSH-conjugation, dichlorovinyl glutathione and dichlorovinyl cysteine are the products usually detected.

Finally, owing to its potential toxicity for human, TCE has been classified in group 1 compounds by the IARC (International Agency for Research on Cancer), indicating that it is certainly carcinogenic to human[14].

1.3 Environmental legislation

One of the most important EU legislation concerning the protection and management of water is defined by the Water Framework Directive 2000/60/EC[15]. Italy has implemented the Directive by the Legislative Decree 152/2006 "Norms Concerning the Environment", usually called "Single Environmental Text". This document regroups in a single legislative text the environmental laws previously contained in several decrees.

At present, the maximum Cl-VOCs water concentration are reported in the Legislative Decree 30/2009[16]. This document was implemented from the Framework Directive 2006/118/EC. In this text the maximum groundwater contaminant levels for TCE and PCE (perchloroethylene or

tetrachloroethylene) are fixed at 1.5 and 1.1 ppb respectively. Concerning U.S., the maximum contaminant levels for TCE and PCE are both fixed at 5 ppb[17].

1.4 Remediation techniques for DNAPLs polluted sites

The physical and chemical properties of DNAPLs, including their relatively low solubility, high specific density and the attitude to remain sorbed to organic materials, make their removal from polluted sites extremely difficult. Therefore, remediation of DNAPLs contaminated sites is a particularly challenging problem.

Remediation technologies are usually classified as non-destructive and destructive as reported in figure 1.3[2].

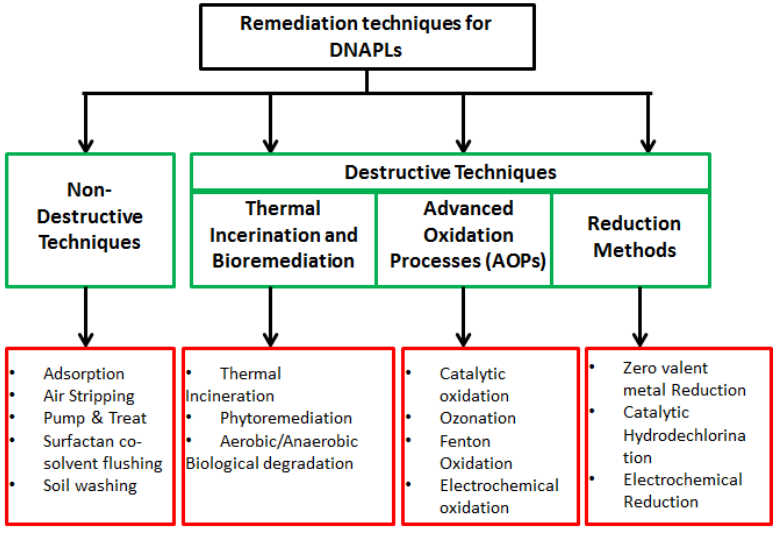

Figure 1.3 Summary of actual remediation methods for DNAPLs

Non-destructive technologies take advantage of the physicochemical properties of the contaminants, such as the high hydrophobicity and the low vapor pressure, for their physical removal from the contaminated sites[9,18,19]. Examples of non-destructive techniques are air stripping, adsorption methods, soil washing, pump & treat (P&T) and surfactant co-solvent flushing[5,20].

Non-destructive techniques are quite efficient in removing DNAPLs from a specific site, however, by using these techniques, the pollutant is simply translocated from one compartment to another. Thus, destructive methods were found to be more attractive for remediation of DNAPLs polluted sites. In the case of chlorinated compounds, these technologies permit the complete destruction of the pollutants by breaking the C-Cl bond, ultimately changing the nature (and the harmfulness) of the compounds.

Bioremediation and phytoremediation are biological approaches where the pollutant could be metabolized by plants and microorganisms during their natural activities[6,21,22].

Thermal incineration was, by far, the most used technology, but it showed high costs related to the operative temperature, often higher than 700 °C, and limitations connected to the chlorinated by-products formation[23].

Advanced Oxidation Processes are a group of chemical treatments designed to eliminate DNAPLs by oxidation reactions; examples are catalytic and photocatalytic oxidation, fenton oxidation, ozonation and electrochemical oxidation[7,24,25].

Finally, reduction methods such as zero-valent metal reduction and catalytic hydrodechlorination are effective techniques for the DNAPLs elimination[26].

Based on the location where the clean-up action is performed, remediation strategies are generally classified in two principal classes, known as *in-situ* and *ex-situ* methods[27].

In-situ technologies treat pollutants directly on-site. *Ex-situ* technologies require the dislocation of the polluted matrix (soil or groundwater) from a contaminated site to a specifically equipped workplace prior the remediation treatment.

In-situ and *ex-situ* techniques show specific advantages and disadvantages shortly resumed in figure 1.4.

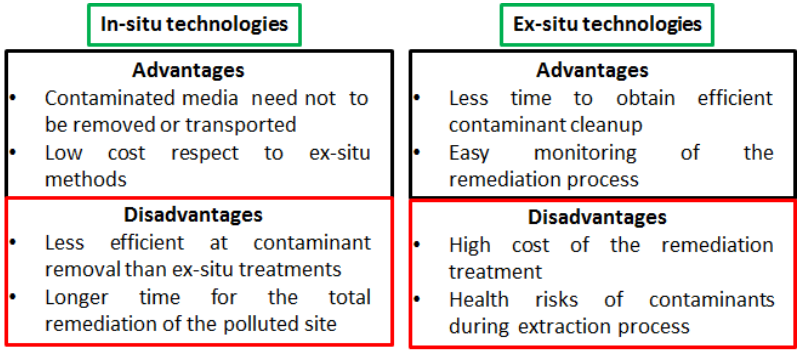

Figure 1.4 Advantages/Disadvantages of Ex-situ/In-situ technologies

In the next chapters, the technologies investigated during this PhD projects will be discussed in details, with a focus on the improvements achieved with respect to the state of the art.

1.5 State of the art in management of contaminated sites

In 2016, in Italy, the official number of polluted areas, known as SIN (Sites of national interest) were 40 (Tab 1.1); 30% of these sites resulted contaminated by DNAPLs, mainly TCE and PCE[28].

Table 1.1 Italian contaminated sites at 2016

Region	N. of sites	Area (1×10^4 m^2)		
		Soil	Water	Total
Piemonte	4	110151	0	110151
Valle d'Aosta	1	23	0	23
Lombardia	5	3752	0	3752
Trentino-Alto Adige	1	24	0	24
Veneto	1	1621	0	1621
Friuli	2	714	1196	1910
Liguria	2	2113	167	2280
Emilia-Romagna	1	25	0	25
Toscana	4	1457	5339	6796
Umbria	1	655	0	655

Marche	1	108	1165	1273
Lazio	1	Currently under investigation		
Abruzzo	1	232	0	232
Campania	2	1083	2886	3969
Puglia	4	10465	13458	23923
Basilicata	2	3645	0	3645
Calabria	1	874	1448	2322
Sicilia	4	7488	16910	24398
Sardegna	2	21625	35164	56789
Italia	**40**	**166055**	**77733**	**243788**

Solofra, Melfi, Biella, Gaglianico, Ternate, Rho and Gardone Val Trompia are only few recent examples of soil and ground-water sites polluted by DNAPLs[29-31].

Bioventing, thermal treatment, soil excavation and phytoremediation are the most common techniques used for the clean-up of contaminated soils, whereas bioventing and P&T are the most commonly employed technologies for groundwater[28].

Fig. 1.5 reports the remediation technologies applied in the EU-surveyed countries as percentages of number of sites per type of treatment.

A recent report published by U.S EPA (United States Environmental Protection Agency) showed that TCE has been found in at least 60% of the US contaminated sites; moreover is the most frequently detected organic contaminant in the

groundwater[32].

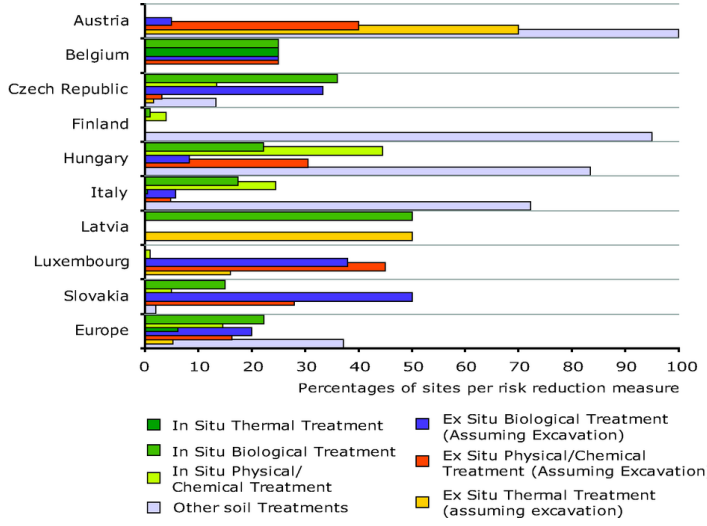

Figure 1.5 Remediation technologies most used in Europe

The most important US TCE polluted site is located in Valmont (Pennsylvania), where a former upholstery manufacturing plant is the main cause for the groundwater pollution.

An important amount of private and public funds has usually spent for the management of the contaminated sites.

In Europe, for example, the 35% of the average remediation budget comes from public funds. Fig. 1.6 shows the estimated allocation of public and private costs for the management of the polluted sites[33].

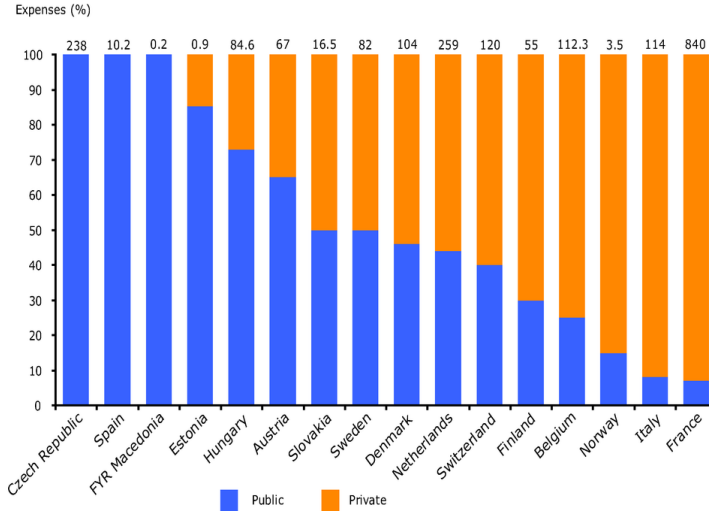

Figure 1.6 Estimated allocation of public and private costs for management of contaminated sites by country. Values on top indicate total annual cost in million euro

References

(1) Schwille F. et al., Lewis Publishers, **1988**
(2) Bimbin H. et al., *Environ. Intern.* **2014**,71,118–138
(3) Miller D.J. et al., *J. Chem. Eng. Data*. **2000**,45,78–81
(4) Wuana R.A.. et al., *African J. Gen. Agri*. **2010**,6,275–287
(5) Intiso A. et al., *Submitted tensioattivi*, **2017**,
(6) Moccia E. et al., *Environ. Sci. Pollut. Res.* **2017**,24,11053-11060
(7) Aranzabal A. et al., *Chem. Pap.* **2014**,68,1169–1186
(8) Doherty, R.E., *Environ. Forensics.* **2000**,1,69–81
(9) Rossi F. et al., *Aiche J.* **2015**,61,3511-3515
(10) U.S.EPA.External review draft. EPA/600/P-01/022A , **2001**
(11) U.S.EPA.,www.epa.gov/teach/chem_summ/TCE_summary.pdf, **2007**
(12) ASTDR, Draft toxicological profile for trichloroethylene, **2015**
(13) Chiu, W.A. et al., *Environ. Health. Perspect.* **2012**,121,303–311
(14) Caldwell J. et al, *IARC Monographs*. **2014**,106,1–514
(15) European Framework Directive 2000/60/EC
http://eur-lex.europa.eu/resource.html?uri=cellar:5c835afb-2ec6-4577-bdf8-756d3d694eeb.0004.02/DOC_1&format=pdf
(16) Italian Legislative Decree 30/2009, http://www.isprambiente.gov.it/files/sostanze-pericolose/d.-lgs.-30-2009.pdf/view
(17) Moran M. et al., *Environ. Sci. Technol.* **2007**,41,74–81
(18) Li B. et al., *J. Environ. Eng.* **2012**,138,903–914
(19) Wei Z. et al., *J. Hazard. Mater.* **2010**,181,147–53
(20) Yang J.S. et al., *J. Ind. Eng. Chem*. **2009**,15,777–779
(21) Justicia-Leon S.D. et al., *Environ. Sci. Technol.* **2014**,48,1851–1858
(22) Chan C.C. et al., *Environ. Sci. Technol.* **2012**,46,10154–10160
(23) Cucciniello R. et al, *Appl. Catal. B: Environ.* **2017**,204,167-172
(24) Blanch-Raga N. et al., *Appl. Catal.B: Environ.* **2016**,187,90–97
(25) Tsai T.T. et al., *J. Environ. Eng.* **2010**,136,288–94
(26) Meshesha B.T. et al., *Appl. Catal. B: Environ.* **2012**,117-118,236–245
(27) Kuppusamy S. et al., *Rev Environ Contam Toxicol* **2016**,236,117-192
(28) Carrabba G., APAT document, http://www.isprambiente.gov.it/contentfiles/00002100/2158-carrabba.zip/view
(29) Dossier Legambiente, http://legambiente.campania.it/beta/wp-content/uploads/2016/02/Solofra_dossier.pdf, **2016**
(30)ARPA document, https://www.arpa.piemonte.gov.it/.../biella/siti../Tetracloroetilene, **2011**
(31)Eupolis document, www.eupolis.regione.lombardia.it/.../00_Ter13010_RFinale.pdf, **2015**
(32) US EPA, Superfund http://www.epa.gov/superfund
(33) EEA document, https://www.eea.europa.eu/.../progress-in-management-of-contaminated-sites/progress, **2007**

CHAPTER II: TCE transport mechanism in water

2.1 Diffusion processes

The physical and chemical properties of DNAPLs are responsible of their stratification at the bottom of the groundwater and aquifer reservoirs, often forming a source of pollution to surrounding media for an extended period of time[1]. Figure 2.1 shows a plausible scenario after the spill of DNAPLs into the soil which subsequently moves vertically under both the forces of soil capillarity and gravity[2-4].

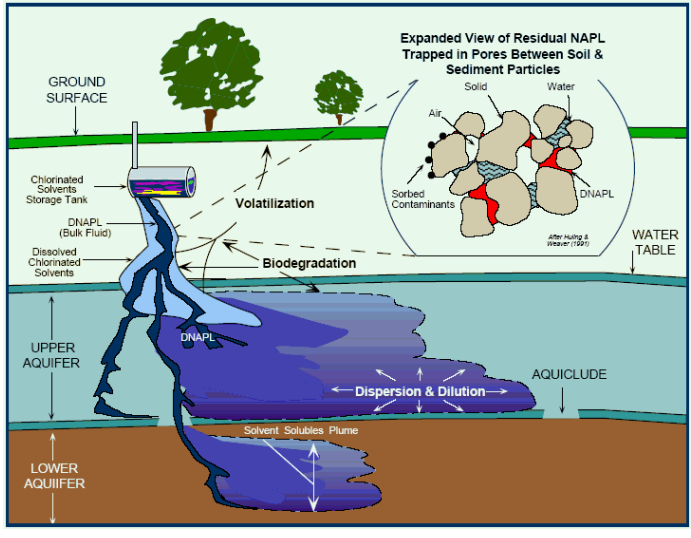

Figure 2.1 Migration of DNAPLs from the releasing area and subsequent contamination of soils and ground water

The knowledge of the fate and the transport of DNAPLs in the subsurface is essential for the environmental risk assessment, for the ecological restoration and for the wastewater

treatment. Several variables such as, DNAPL characteristics, subsurface media characteristics and saturation dependent parameters influence the fate and the transport of DNAPLs.

In the last few years several environmental diffusion models based on Taylor and Aris advection-dispersion methods[5] were developed to predict the fate of DNAPLs before and during the remediation procedure[6-8]. In these models, the dispersion coefficients are a function of the molecular diffusivity of the DNAPLs in water and of the mechanical dispersion due to the water flows. Moreover, the accurate evaluation of the mass transfer coefficients associated with the dissolution of DNAPL pools and ganglia in the subsurface environment is also strongly dependent on the pollutants diffusion coefficients.

Diffusion in liquids plays an important role in many chemical and biochemical processes, and it determines the rate of mass transfer in many systems, both natural and industrial. An accurate measurement of diffusion coefficients is therefore desired but often, especially in multicomponent systems, it represents a nontrivial problem to overcome. For example, a ternary system (two solutes in a solvent) has four diffusion coefficients, including the main (D_{ii}) and the cross (D_{ik}) diffusion terms, which form the diffusion matrix **D:**

$$\mathbf{D} = \begin{bmatrix} D_{11} & D_{12} \\ D_{21} & D_{22} \end{bmatrix}$$

D_{ii} represent the molecular diffusion of an i^{th} component due to a gradient in its own concentration, while the cross terms D_{ik} take into account the influence of the flux of one component on the motion of the others, and they can be large and be positive or negative, thus having a substantial effect on flows of matter.

Diffusive processes in solutions containing an arbitrary number N of solutes can be described by Fick's diffusion equation and continuity equation:

$$J_i = -\sum_{k=1}^{N} D_{ik} \nabla c_k \qquad i = 1, \ldots, N \qquad (1)$$

$$\nabla J_i = -\frac{\partial c_i}{\partial t} \qquad (2)$$

where J_i is the flux of the i^{th} component and c_k is the concentration of the k^{th} component. As above mentioned, D_{ii} and D_{ik} are the main and the cross diffusion coefficients. Using equations 1 and 2 it is possible to follow the rate of concentration change of a component in unsteady diffusion processes.

In the specific case of TCE, the value of the main diffusion coefficient used in models ($D_{\mathrm{TCE}} \approx 1 \times 10^{-5}$ cm^2 s^{-1} at 25°C) is a

theoretical estimation, generally derived from the well-known Wilke and Chang (W&C) equation

$$D = \frac{7.4 \cdot 10^{-8} (xP_M)^{0.5} T}{\eta V^{0.6}} \qquad (3)$$

where the diffusion coefficient expressed in $cm^2\ s^{-1}$ is a function of the association parameter, x, of the molecular weight of the solvent, P_M (g mol^{-1}), of the temperature, T (K), of the viscosity of the solution, η (cP), and of the molal volume of the solute at normal boiling point, V ($cm^3\ mol^{-1}$)[9]. In addition to the W&C equation, another commonly used relation is the Hayduk e Laudie (H&L) equation. Hayduk e Laudie developed a specific relation for the diffusion of solutes in water; by eliminating the solvent-specific parameters and the explicit dependence on the absolute temperature from the W&C equation, they obtained

$$D = 13.26 \cdot 10^{-5}\ \mu_B^{-1.14}\ V_A^{-0.589} \qquad (4)$$

In this case the diffusion coefficient D ($cm^2\ s^{-1}$) is a function of the viscosity of the water μ_b (cP) and of the the LeBas molar volume V_A ($cm^3\ mol^{-1}$) of the solute at the boiling point[10,11].

Several techniques could be used to measure diffusion coefficients. Among these methods, diaphragm-cell and

conductimetric techniques are reliable and well established, but they are also very time-consuming and rarely used anymore[12-16]. Though highly accurate, Gouy and Rayleigh optical interferometric techniques are elaborate and subjected to gravitational instabilities and convection[17,18]. Moreover, they are laborious and require highly specialized experimentalists.

As previously mentioned, to study the fate of TCE in water and to devise effective remediation strategies, a series of advection-diffusion (dispersion) models, where the diffusion coefficient of TCE (D_{TCE}) is an important parameter, have been developed.

However, at best of our knowledge, D_{TCE} has never been determined experimentally, probably because TCE is only slightly soluble in water and its volatility makes difficult the preparation of stable standard solutions.

In this context, we designed a method based on the Taylor Dispersion Analysis (TDA) which allow to measure D_{TCE} in a broad range of temperature and, in principle, in any solvent[19]. Also, from the temperature dependence of D_{TCE}, it was possible to calculate the specific fitting constant for TCE in the W&C equation and the activation energy of the diffusion process through the Arrhenius plot.

2.2 Taylor Dispersion Analysis

The TDA is a fast and reliable method for measuring the diffusion coefficients of solutes in one or multi-components solutions[20]. The original treatment of the dispersion problem was developed by Taylor and Aris[21,22]. Successively Wakeham et al. revised and improved the theory and developed an ideal equipment to measure mutual diffusion coefficients[23,24]; the apparatus they designed consisted in standard liquid chromatographer equipped with a dispersion column in the place of the classic separation one. Since then, the technique has been rapidly developed and used to measure diffusion coefficients for hundreds of different systems.

Though less precise with respect to other techniques, the TDA presents several advantages such as a simpler experimental apparatus, a small concentration difference between the sample and the solvent and the absence of a calibration procedure.

The TDA is based on the diffusive spreading of a pulse of solution injected into a laminarly flowing stream of the same mixture but with slightly different concentration (Fig. 2.2). A small volume of the perturbing solution is injected into the flowing eluent at the entrance of a long capillary tube (the dispersion column). As it moves along the tube at a constant speed, the injected sample is deformed by the shear flow, the

rate of which has a parabolic shape across the capillary, and by radial diffusion.

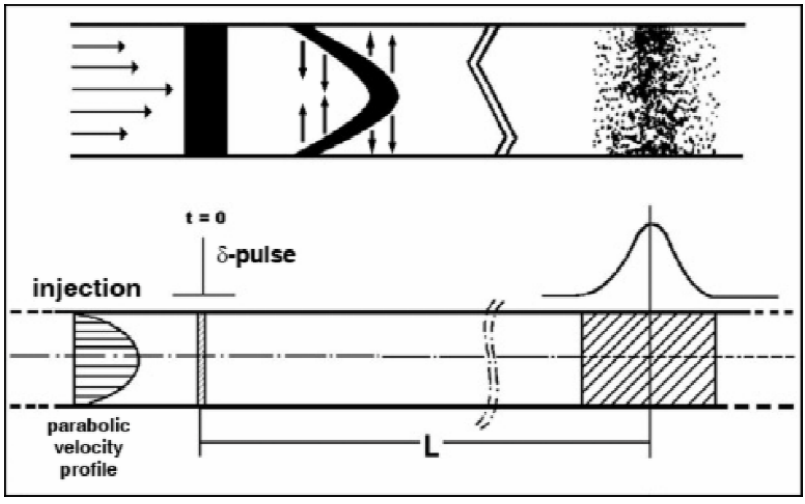

Figure 2.2 A small volume of solution *(δ-pulse)* is injected into a laminar carrier stream at the entrance to a long capillary tube. The injected sample is deformed by the flow in a parabolic shape, then due to the radial diffusion it spreads out into a nearly Gaussian distribution as it flows along the tube. Diffusion coefficients are calculated from the shape of the eluted peak which is monitored by a suitable detector such as a flow-through spectrophotometer or refractometer

The eluted peak, sometimes called the Taylor peak, is monitored by a suitable detector such as a refractive index detector (RID). The diffusion coefficients are calculated from the parameters of the Gaussian functions that fit the eluted peak.

Taylor demonstrated that if the elution process is slow enough, the radial variation of the sample concentration is small relative to the axial variation, and the concentration

profile of the *i*th species (c_i) in a *n*-component system can be described with a one-dimensional equation (c_i is averaged over the cross section of the tube) having the form

$$\frac{\partial c_i}{\partial t} = \sum_{j=1}^{n} F_{ij} \frac{\partial^2 c_j}{\partial z^2} \tag{5}$$

where

$$F_{ij} = \frac{R_0^2 u_0^2}{48 \det(\mathbf{D})} \det(\mathbf{M}_{Dji})(-1)^{(i+j)} \tag{6}$$

det(**D**) is the determinant of the $n \times n$ diffusion matrix **D** and det($\mathbf{M}_{Dji}$) is the determinant of the minor associated with element D_{ji} of $\mathbf{D}$[21,25]. The coefficients F_{ij} have the same dimensions as the diffusion coefficients D_{ij} ($cm^2\ s^{-1}$), but they are inversely proportional to D_{ij}. In the simplest case (one solute and one solvent), when all the off diagonal elements of **D** are zero, Eq. 6 reduces to $F_{ii} = K_{FD}/D_{ii}$, where $K_{FD} = R_0^2\ u_0^2 / 48$. The F_{ij} and D_{ij} parameters are can be found by fitting all the experimental peaks *v(t)*.

In our experimental system, composed by one solute and the solvent, the experimental Gaussian peaks can be fitted by the following equation:

$$v(t) = \frac{P_{\exp}}{\sqrt{4\pi F t}} \exp\left[-\frac{u_0^2 (t - t_0)^2}{4Ft} \right] \tag{7}$$

In principle, *F* can be retrieved by fitting just one

experimental peak through Eq. 7, however, the simultaneous fitting of multiple experimental peaks improve the confidence on the value of *F*. Finally, *D* can be easily calculated through the formula

$$D = \frac{R_0^2 \, u_0^2}{48F} \tag{8}$$

2.3 Experimental Section

Our experimental setup for the measurement of diffusion coefficients consists of a high pressure liquid chromatography apparatus (Agilent 1260 series), which ensures suitable experimental conditions for the Taylor dispersion measurement. The length of silica glass capillary used in all the experiments was 15 m between the injector and the cell of the differential flow-through thermostated refraction index detector, RID. The inner radius R_0 (0.016 ± 0.02 cm) of the tubing was checked by gravimetry, that is, from the mass of water required to fill the tube and it was found to be consistent with the value declared by the manufacturer. Both untreated and deactivated silica capillaries (SUPELCO Analytical) were employed. To adapt the small bore silica tubings to the standard 1/16″ connection ports of the HPLC apparatus, a specifically designed microtight fittings (IDEX

UP-CHURCH) were used. The tubing was coiled in a 30-cm diameter helix and immersed in a thermostated water-bath (Julabo ME-16G). For all the experiments, the temperature of the water-bath was set as to match that of the RID cell (Agilent G1362A). An isocratic pump (Agilent G1310B), which maintained a steady flow, was placed between the eluent reservoir and the injector. A 2-μL sample loop was used for injection. The detector was connected to a personal computer for data acquisition. An inline ion exchange resin-based degasser (Agilent G1322A) was also placed between the eluent reservoir and the pump.

Solutions were prepared using bidistilled water, TCE (Sigma-Aldrich analytical grade), mannitol (Sigma analytical grade), and sodium chloride (Sigma analytical grade). TCE was handled only with glass tools and syringes.

Samples were injected every 20 min to avoid the overlapping of the peaks. Experimental peaks generated with different injections were simultaneously fitted, using the Levenberg–Marquardt algorithm, to Eq. 7[26]. F and t_0 were fitted as shared parameters among the multiple peaks, P_{exp} was fitted as single parameter for each peak, while μ_0, calculated from the instrumental flow rate, f ($cm^3\ min^{-1}$) and from the capillary radius, R_0, was taken as a constant input parameter. A baseline of the form ($a + bt$) was previously subtracted from the

recorded signals with the help of a suitable software.

2.4 TCE diffusion coefficient in water

Generally, the most used capillaries for the implementation of the Taylor method are made in Teflon. However, TCE is known to have a great affinity for this material[27] and its sorption on the tubing walls during the dispersion process alters the measurement of the diffusion coefficients. The physicochemical properties of TCE, in particular its high volatility and its affinity for polymeric materials, make difficult the choice of an alternative material. Silica tubings used as columns for gas chromatography seemed to be a valid alternative and we successfully used them for the measurement of D_{TCE} in water. We adapted silica capillaries (O.D. 430 μm) to the standard conic 10–32 HPLC ports using nanotight adapters and we carefully conducted calibration procedures in several experimental conditions.

In particular, the diffusion coefficients in water of a strong electrolyte, NaCl, and a sugar, mannitol, were measured. Both the chemicals were tested in deactivated and untreated columns to check whether the polarity of the capillary could have an influence on the dispersion processes. The two diffusion coefficients were found to differ less than 1% with respect to those determined by diffractometer methods in all

the experimental conditions[28,29].

Figure 2.3 shows the dispersion peaks of TCE obtained for two different initial concentrations of the samples injected in a flowing solution of [TCE]= 1×10^{-4} M in water at 30°C.

Solid lines represent the best fitting curves of the experimental data obtained by means of Eq. 7, after the subtraction of the signal baseline. The two peaks were fitted simultaneously and the integration confirmed a linear dependence of the instrument response on the concentration of the injected samples.

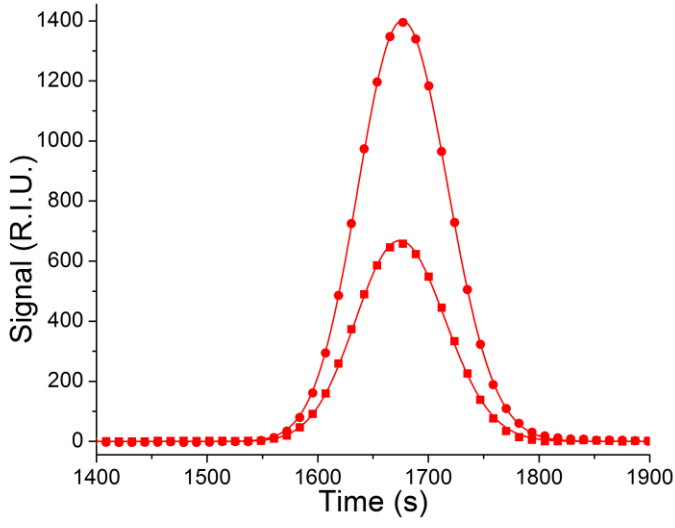

Figure 2.3 Experimental peaks obtained by injecting a solution with Δ[TCE] = 1×10^{-3} M (•) and with Δ[TCE] = 2×10^{-3} M (•), in a flowing solution with [TCE]=1×10^{-4} M. Solid lines represent the best fitting curves

Peaks generated by injections at various Δ[TCE] were simultaneously fitted in order to minimize the experimental

errors and results for different experimental temperatures are reported in Table 2.1 and in Figure 2.4.

Table 2.1 Dependence of D_{TCE} upon the temperature in water solution

T (°C)	D_{TCE} ($cm^2\ s^{-1}$)
25	$8.16 \pm 0.06 \times 10^{-6}$
30	$9.48 \pm 0.06 \times 10^{-6}$)
35	$1.08 \pm 0.02 \times 10^{-5}$
45	$1.27 \pm 0.08 \times 10^{-5}$
55	$1.54 \pm 0.01 \times 10^{-5}$

The concentration of TCE in the eluent solution was varied in the range 1×10^{-5}–1×10^{-4} M without finding any appreciable difference among the diffusion coefficients measured at different temperatures, this means that for diluted solutions D_{TCE} is independent from the concentration of TCE.

These results suggest that over the range of concentrations studied, the TCE molecules move through water more or less independently of each other.

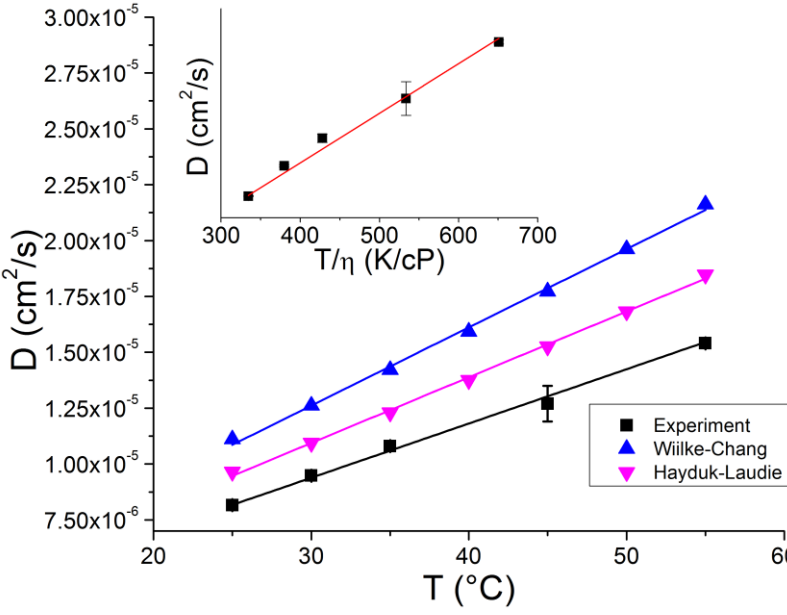

Figure 2.4 Comparison among experimental and theoretical data for D_{TCE} The inset reports the dependence of D_{TCE} upon the ratio T/η from the W&C equation

When the concentration of TCE in the flowing solution is rather small and does not contribute significantly to the viscosity of the eluent, diffusion coefficients increase linearly with the temperature as predicted by the semiempirical relation of Wilke and Chang (Eq. 3) and Hayduk e Laudie (Eq. 4). The comparison among experimental and theoretical values is reported in Figure 2.4. The up-pointing triangles represent the theoretical values for D_{TCE} calculated by the W&C relation, where the typical values for the water as the solvent (P_M, η, and x=2.6) were used and the molar volume

for TCE, V = 96.3 cm^3 mol^{-1}, was calculated using the incremental method of Le Bas corrected by a factor 0.9[9,11,30,31].

The down-pointing triangles represent the values for D_{TCE} calculated through the H&L relation with V_A = 107 cm^3 mol^{-1}. Both the theoretical series resulted overestimated (20–40%) with respect to the experimental diffusion coefficients determined in this work (black squares in Figure 2.4). The inset in Figure 2.4 shows the dependence of D_{TCE} respect to the ratio T/η, the linear fitting of the plotted data, scaled by the ratio $(xP_M)^{0.5}/V^{0.6}$, yielded the numeric constant of the W&C relation for the specific case of TCE (5.1×10^{-8} in the place of 7.4×10^{-8}), so that theoretical values can be extrapolated for every temperature.

The dependence of D_{TCE} upon the temperature (Figure 2.5), allowed to calculate the activation energy for the diffusion process E_a (Kcal mol^{-1}) of TCE in water, through the Arrhenius relation

$$\ln D = \ln D_0 - \frac{E_a}{RT} \qquad (9)$$

where D_0 (cm^2 s^{-1}) is the diffusion coefficient for infinite temperature, R is measured in J mol^{-1} K^{-1} and T in K. The result (4.1 ± 0.1 Kcal mol^{-1} with D_0 =8.9×10^{-3} cm^2 s^{-1}) was found to be in line with the literature data and lies in between

the value for hydrocarbons and aromatic compounds[32,33]. The inset in Figure 2.5 also reports the linear dependence of D_{TCE} on the shear viscosity of the solutions at different temperatures.

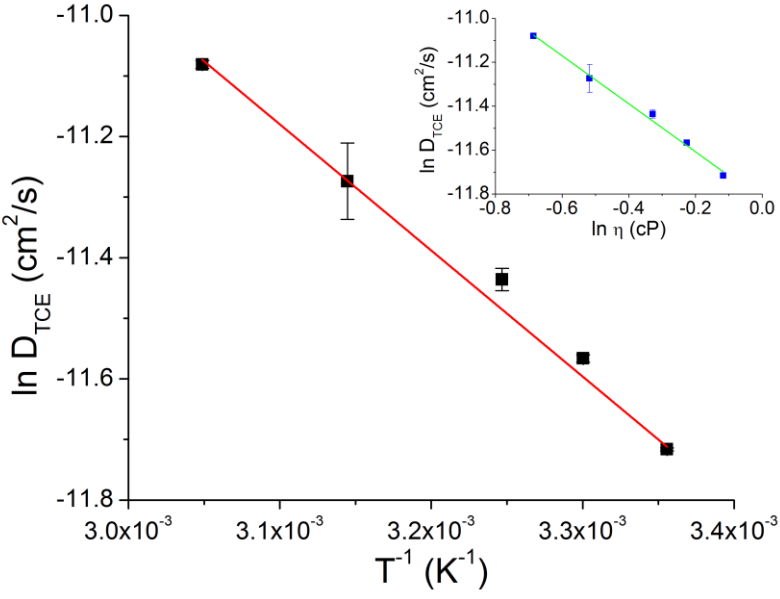

Figure 2.5 Arrhenius plot of D_{TCE} vs. 1/T. The inset reports the dependence of D_{TCE} on the shear viscosity of solutions at different temperatures

2.5 Conclusion

In the first part of this PhD thesis, we worked on the diffusion mechanism of TCE in water. In particular, we developed an easy way, based on the Taylor Dispersion Analysis, to measure for the first time the TCE diffusion coefficient in water. In principle, this method could be applied to all those

chemicals, which present experimental difficulties, such as high volatility or high affinity for commonly used polymeric materials. In the specific case of TCE, we found that at 25°C $D_{TCE} = 8.16 \pm 0.06 \times 10^{-6}$ cm^2 s^{-1} and the value was found to increase linearly with the temperature, while, in the limit of the experimental error, was independent from [TCE] for dilute solutions. Moreover, from the temperature dependence of the diffusion coefficients we could modify the Wilke and Chang equation to adapt it to the specific case of TCE, thus providing a suitable tool to extrapolate D_{TCE} for any desired experimental temperature.

The above reported results are important to improve the advection dispersion models usually used to understand the fate of TCE during the remediation procedures.

References

(1) Russell H.H., Ann Arbor Press, **1996**
(2) Hunt J.R., *Water Resour. Res.* **1988**,24,1247–1258
(3) Vesper D.J. et al., *Theor. Appl. Karstol.* **2000**,13,63–73
(4) Budroni M. et al., *Chaos.* **2015**,25,064502
(5) Taylor G., *Proc. R. Soc. London A.* **1953**,219,186–203
(6) Chen G.Q. et al., *Ecol. Model.* **2010**,221,2927–2937
(7) Wu Z. et al., *Ecol. Model.* **2011**,222,456–474
(8) Zeng L. et al., *Commun. Nonlinear Sci. Numer. Simulat*. **2011**,16,206–215
(9) Wilke C.R et al., Chang P. *AIChE J.* **1955**,1(2),264–270
(10) Hayduk W. et al., *AIChE J.* **1974**,20(3),611–615
(11) Le Bas G., Longmans, Green, London, **1915**
(12) Tyrrell H.J.V. et al., Butterworths, London, **1984**
(13) Leaist D.J. , *Faraday Trans. I*. **1987**,83,829-839
(14) Noulty R.A. et al., *J. Phys. Chem.* **1987**,91,1655-1658
(15) Leaist D.J., *Can. J. Chem.* **1985**,63,2933-2939
(16) Leaist D.J. et al., *Can. J. Chem.* **1985**,63,476-482
(17) Fujita H. et al., *J. Am. Chem. Soc*. **1956**,78,1099-1106
(16) Leaist D.J. et al., Can. J. Chem. **1985**,63,476-482
(17) Fujita H. et al., *J. Am. Chem. Soc.* **1956**,78,1099-1106
(18) Fujita H. et al., *J. Phys. Chem.* **1960**,64,1256-1263
(19) Rossi F. et al., *Aiche J.* **2015**,61,3511-3515
(20) Rossi F. et al., *J. Phys. Chem. B* **2010**,114,8140–8146
(21) Taylor G., *Proc. R. Soc. London A.* **1954**,473-477
(22) Aris R., *Proc. R. Soc. London A.* **1956**,235,67–77
(23) Alizadeh A. et al., *Int. J. Thermophys.* **1980**,1,243–284
(24) Alizadeh A. et al., *Int. J. Thermophys.* **1982**,3,307-323
(25) Vanag V.K. et al., *J. Phys. Chem. B.* **2008**,112,9058–9070
(26) Gill P.E. et al., *J. Numer. Anal.* **1978**,15,977–992
(27) Regan F. et al., *Vib Spectrosc.* 1997,14, 239–246
(28) Cussler E.L., Cambridge University Press, **2009**
(29) Dunlop P.J., *J. Phys. Chem.* **1965**,69,4276–4283
(30) Poling B.E.et al., New York: McGraw-Hill Professional, **2000**
(31) Gulliver J.S. New York: Cambridge University Press, **2007**
(32) Witherspoon P.A. et al., *J. Phys. Chem.* **1965**,69,3752–3755
(33) Bonoli L. et al., *J. Phys.Chem.* **1968**,72,2532–2534

CHAPTER III: Removal techniques from groundwater and soils polluted by TCE

3.1 Employment of a biodegradable surfactant for groundwater remediation

3.1.1 Surfactant/co-solvent flushing

Surfactant co-solvent flushing technique is an improvement of P&T technology; in this method a mixture of chemicals is generally employed to enhance the mobility of DNAPLs and, consequently, increase the extraction yield[(1)].

As for P&T method, the system consists of a series of injection and extraction wells to hydraulically sweep the contaminant plume (Fig. 3.1)[(2)]. The injected fluid promotes the DNAPLs solubilization and mobilization by lowering the interfacial tension with the contaminant in the aqueous phase.

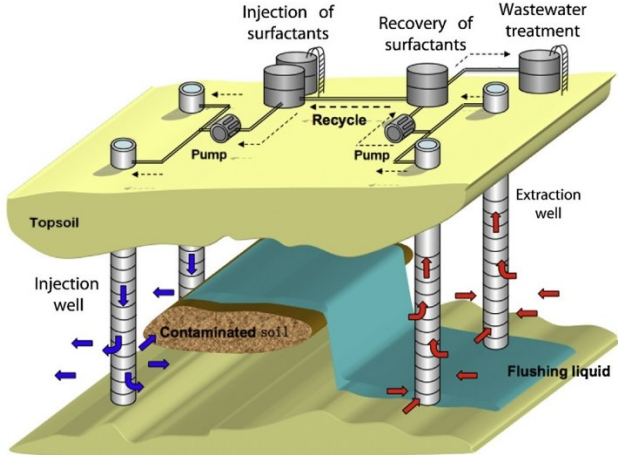

Figure 3.1 Surfactant co-solvent flushing scheme

The groundwater and the elutriate (a mixture of contaminant and injected solution) are, therefore, brought through extraction wells to the surface. Afterwards, both are treated and reinjected into the system or discharged. The injected fluid is usually a mixture of more reagents (surfactant, alcohol etc.), which are miscible or partially soluble in the aqueous phase.

The advantages and limitations of surfactant co-solvent flushing technique are summarized in Figure 3.2[1].

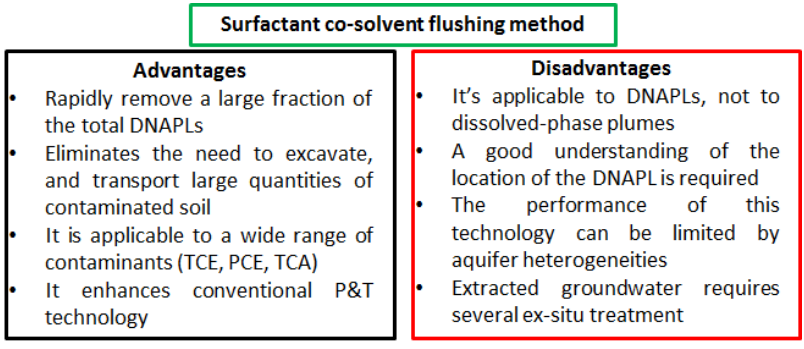

Figure 3.2 Advantages and limitations of surfactant co-solvent flushing technology

3.1.2 Applications of surfactants to remediation processes: an overview

Surfactant molecules generally consist of a hydrophilic head of various nature (ionic or non-ionic) and a hydrophobic tail which is usually linear or branched, with or without unsaturations[3].

In a groundwater polluted site, surfactant properties may be used to mobilize residual DNAPLs into the mobile flushing solution[1]. Solubilizing surfactant flooding and mobilizing surfactant are the two principal mechanisms that can be used for DNAPLs removal. In the first approach, surfactant is able to increase the aqueous solubility of the pollutant due to the contact with the DNAPLs. In the second approach, the reduction of contaminant-water interfacial tension allows to promote the physical mobilization of DNAPLs. The choice of an appropriate surfactant influences the ratio of the two mechanisms occurring in the injected liquid.

Generally, surfactants consist of two traditional categories based on the hydrophilic group: ionic that include cationic, anionic and zwitterionic, and nonionic surfactants[4]. In addition, in the last few years, biosurfactants have also been tested for green remediation purposes. Respect to traditional surfactants, biosurfactants exhibit many advantages such as environmental compatibility, low toxicity, high biodegradability, in addition to efficiency in extreme pH, temperatures and salinity conditions[5]. However, the high production costs and the relatively low availability still limit the employment of biosurfactants for field applications[5,6].

Table 3.1 summarizes some recent works reporting the use of surfactants for the remediation of soil and water contaminated

by DNAPLs, in particular TCE.

Table 3.1 Application cases of different surfactants for the remediation of contaminated sites

Surfactant	Pollutant	Reference
Spolapon AOS	PCBs	(7)
CTAB	Benzene	(8)
SDS	TCE	(9)
SDS, Triton X-100, CTAB, UH Biosurfactant	TCE	(10)
Rhamnolipid, surfactin	TCE, PCE	(11)
AOT/SMDNS mixture	DCE,TCE,PCE	(12,13)
Tergitol NP-10	Diesel	(14)
Tween 80	p-cresol	(15)

In this context, we tested the performances of the surfactant Synperonic 91/5 (Syn 91/5) to improve the aqueous solubility of TCE; being an ethoxylated alcohol (AEs), Syn 91/5 is considered a low-impact and biodegradable "green" surfactant[16]. AEs are a family of synthetic nonionic surfactants that present an hydrophobic alkyl chain linked via an ether bond to an hydrophilic ethylene oxide (EO) fragment and have a typical structure $R(OCH_2CH_2)_nOH$[17]. Owing to many advantages (solubilization capability and low toxicity), AEs are largely employed into the research on remediation of contaminated site[18].

In this project, the dissolution of TCE into water solutions at

increasing [Syn 91/5] was investigated by means of UV-VIS technique, having the TCE a characteristic absorption wavelength at $\lambda = 200$ nm[19].

Syn 91/5 allowed to increase up to 15 times the TCE aqueous solubility. Moreover the dependence of TCE solubility upon temperature variation was also assessed, showing the highest performances for the lowest temperature.

3.1.3 Experimental section

First, the CMC of Synperonic 91/5 was determined with the pyrene 1:3 ratio method[20,21]. This technique takes into account the ratio of pyrene fluorescence intensities corresponding to the first and third vibrational peaks (I_1/I_3). It is well known that the pyrene 1:3 ratio is influenced by the polarity of the solvent and it decreases passing from a hydrophilic to a hydrophobic environment This parameter reaches a minimum constant value above the cmc of the surfactant, as consequence of the pyrene solubilization in the micelles structure.

By following this method, a small aliquot of a methanolic pyrene solution ([pyrene] = 1×10^{-6} M) was mixed with different concentrations of Synperonic 91/5[22]. The fluorescence spectra were recorded with a Varian fluorescence spectrophotometer (Cary Eclipse 130 Series) by

using an excitation wavelength of 334 nm and measuring the intensities emitted at λ_1 = 373 nm and λ_3 = 384 nm. TCE, Pyrene (Sigma Aldrich) and Synperonic 91/5, (Croda) were used as purchased without further purification.

Solubilization studies of TCE in the surfactant solutions were performed by means of a UV-Vis spectrophotometer (Agilent 8453) by measuring the maximum absorption of TCE at λ = 200 nm.

Solutions were prepared by adding known quantities of TCE to a surfactant solution, until the maximum solubility of TCE was reached. The limit of maximum solubility was easily recognizable by the formation of a biphasic microemulsion as shown in figure 3.3.

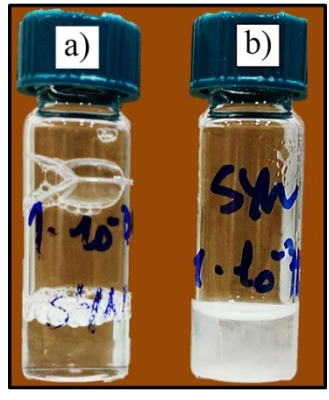

Figure 3.3 Microemulsion with [TCE] = 0.020 M and [SYN] = 1×10^{-3} (left); b) demixed microemulsion with [TCE] = 0.025 M [SYN] = 1×10^{-3} (right)

The prepared samples were diluted 1:100 and introduced in a quartz cuvette prior to the spectrophotometric measurements.

The contribute of the Syn 91/5 to the UV-VIS spectra was removed maintaining the same surfactant concentrations in both cells (reference and measurements). The molar extinction coefficient calculated from the standard curve of TCE in water was 7642 M^{-1} cm^{-1}. This value was used in surfactants solutions to calculate the concentration of the solubilized TCE. The measurements were performed at three different temperatures: 4°C, 20°C, 30°C and at different concentrations of Synperonic, all above the critical micelle concentration.

3.1.4 CMC determination of Syn 91/5 in water

Figure 3.4 reports the plot of the pyrene 1:3 ratio as a function of the logarithm of the total surfactant concentration. As it can be seen, the shape of the curve can be adequately described by a Boltzmann-type sigmoid.

The fitting of the experimental curve allowed to determine the CMC of Syn 91/5 ($6.1 \pm 0.2 \times 10^{-4}$ M), as the center of the sigmoid curve. All details about fitting procedure are reported by Aguiar et al[21]. This results was found in line with those reported for similar AE surfactants[23-27].

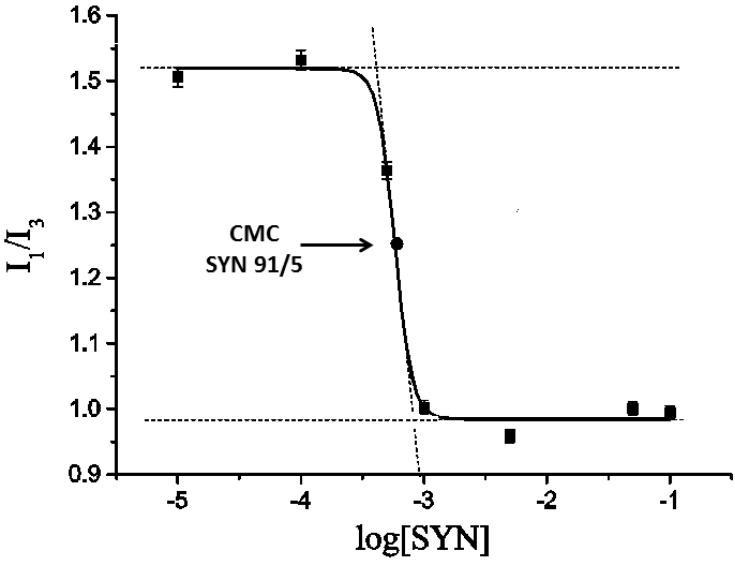

Figure 3.4 Plots of pyrene 1:3 ratio versus logarithm of the [Syn 91/]. The center of the sigmoid corresponds to the CMC of the surfactant

3.1.5 TCE solubilization in Syn 91/5

TCE solubilization studies were performed at three different temperatures (4°C, 20°C, 30°C) in a range of surfactant concentration moving above the CMC up to 1M.

Table 3.2 shows the TCE solubility as a function of [Syn 91/5]. As clearly shown, in the interval $6.1 \times 10^{-4} < [SYN] < 0.1$ M the solubility of TCE only doubled passing from 0.01 M (solubility in water) to 0.02 M for [SYN] = 0.1 M at 20 °C; this is probably due to the short hydrophobic chain of SYN 91/5 that not permitted a relevant increase of TCE solubility when only micelles were present.

Table 3.2 Maximum solubility of TCE at different [SYN 91/5]

[Synperonic 91/5] (mol/L)	[TCE] (mol/L)
1	0.156
0.5	0.111
0.1	0.022
1×10^{-3}	0.020
1×10^{-4}	0.016
0	0.0097

Nevertheless, increasing [SYN] in the range of 0.1-1 M, a strong increment of TCE solubility was observed.

This is related to the formation of a O/W microemulsion, that allowed to drastically improve the aqueous solubility of the pollutant.

The UV-VIS spectra of several solutions (always diluted 1:100 before the analysis), prepared by adding different amount of TCE at a fixed concentration of surfactant ([SYN] = 0.5 M), are reported in Figure 3.5a. The maximum solubility of TCE (≈ 0.1 M), before the phase separation, was observed at the highest absorbance (black line spectra in the figure).

The same procedure was repeated for different [SYN] concentrations in the interval of 0.1-1M and the results (maximum solubility spectrum versus [SYN] concentration) are reported in Figure 3.5b.

As clearly shown, a drastically improvement of TCE

solubility was observed up to 0.7 M,; after, synperonic 91/5 was less efficiency in solubilizing the pollutant, probably due to a shift from a microemulsion phase to a different aggregation structure.

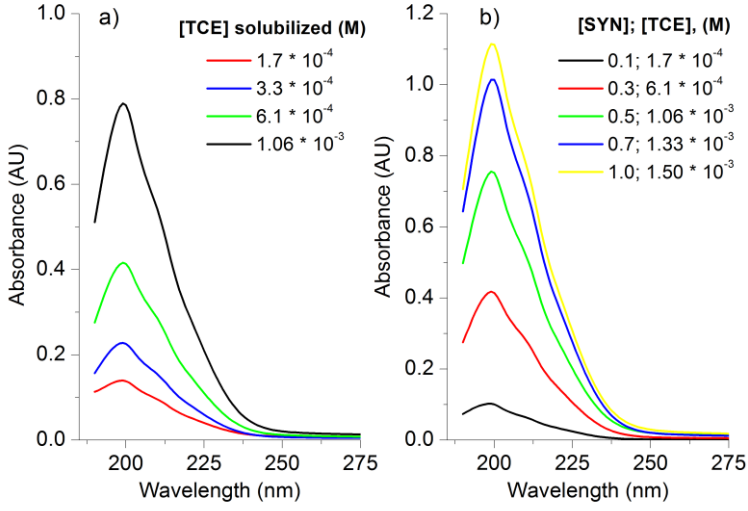

Figure 3.5 a) Absorption spectra of TCE in [SYN] = 0.5 M. b) Absorption spectra of saturated solutions of TCE at different [SYN]. All spectra in a) and b) were taken from diluted solutions (1:100)

Molar solubilization ratio (MSR), expressed in mol/L, and the analogous Weight Solubilization Ratio (WSR), expressed in g/L, are useful parameters to describe the capability of Syn 91/5 to solubilize TCE. The MSR has been defined for micellar systems[10], but it can be adapted to a microemulsion by considering the emulsification concentration in the place of the CMC, as the critical parameter for the solubilization

enhancement:

$$MSR = \frac{Y - Y_0}{X - X_0} \quad (1)$$

where Y is the [TCE] at a specific concentration of surfactant, X, while Y_0 is the [TCE] at the emulsification concentration, X_0[10].

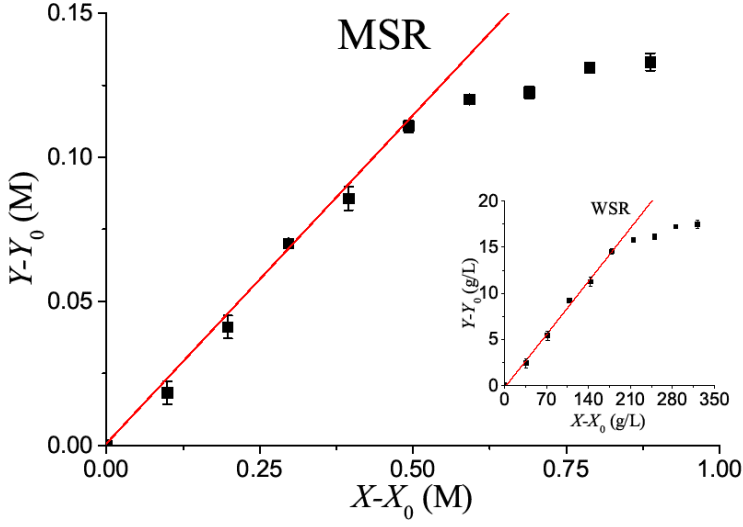

Figure 3.6 MSR and WSR of TCE for Synperonic 91/5 at 25°C

Figure 3.6 shows the solubility curve of TCE, derived from the Figure 3.5b. Based on Eq. 1, MSR was calculated as the slope of the linear part of the solubility curve, obtaining a value of $21 \pm 1 \times 10^{-2}$. By using the same procedure, the value determined for WSR was $85 \pm 4 \times 10^{-3}$ (inset in Fig. 3.6).

For a real application of SYN 91/5 as active agent in

surfactant co-solvent flushing, it is important to evaluate the influence of the temperature on the TCE solubility.

Several tests were performed for [SYN] = 0.1, 0.3, 0.6 and 0.9 M at 4°C and 30°C. The results in term of maximum solubility of TCE, MSR and WSR are reported in Figure 3.7.

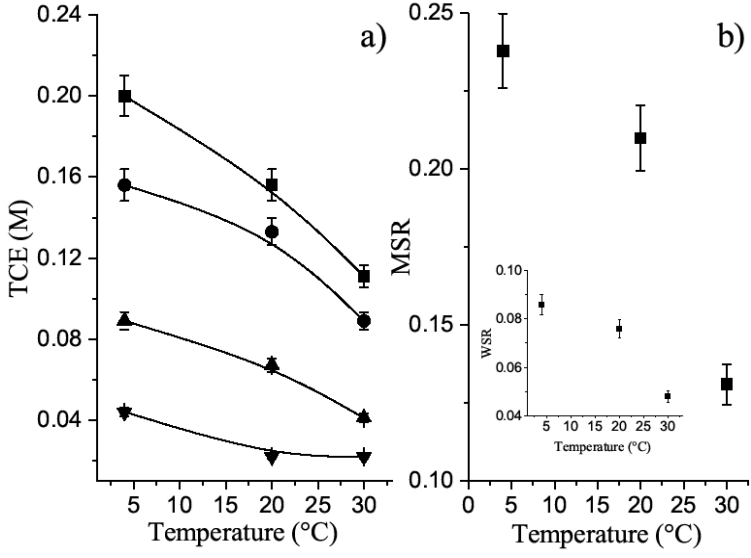

Figure 3.7 a) Maximum solubility of TCE in Syn 91/5 at different temperatures, [SYN]= 0.1 M (▼), [SYN]= 0.3 M (▲), [SYN]= 0.6 M (●), [SYN]= 1 M (■); b) MSR of TCE in synperonic 91/5 at different temperatures, the inset reports the WSR.

As it can be seen, a reduction of the experimental temperature determined an increase in the TCE solubility; for example the solubility of TCE at [SYN] = 0.1 M, was 0.12 M at 30 °C and 0.2 M at 4 °C (Fig. 3.7a). The MSR and WSR also changed accordingly (Fig. 3.7b). This can be related with the

improvement of the microemulsion stability at lower temperatures, as expected, for this class of surfactants[28,29].

3.1.6 Conclusion

In order to improve surfactant co-solvent flushing technologies for the remediation of TCE polluted sites, we investigated the performances of the surfactant Synperonic 91/5 (Syn 91/5) to improve the aqueous solubility of TCE. Syn 91/5 was chosen thanks to its features, that make it an ideal candidate for *in-situ* application.

A relevant enhancement in the TCE solubility was observed for concentrations of surfactant in the interval 0.1-1M, due to the formation of a microemulsion phase. At 20°C, an high TCE solubility (15 times greater respect to pure water) in surfactant solutions ([SYN] = 1 M) was achieved.

The variation of the solubilized TCE with respect to the concentration of the surfactant was found to be linear in the range 0.1–0.7 M. MSR and WSR parameters were calculated from the slope of the linear part of the solubility curve, in order to measure the ability of Synperonic 91/5 in solubilizing TCE.

The temperature plays an important role on the stability of the microemulsion phase, and thus, in the solubilization capability of the surfactant. In particular, it was found that the

maximum solubility of TCE diminished from 0.20 M at 4 °C to 0.111M at 30 °C for [SYN] = 1M.

In conclusion we demonstrated the high performances of Syn 91/5 to improve the aqueous solubility of TCE and how the temperature can influence this remediation techniques. A plausible future work could be the evaluation of a possible employment of Synperonic 91/5 and analogous surfactants for in field application.

3.2 Phytoremediation of trichloroethylene contaminated sites

3.2.1 Introduction

Phytoremediation is an in-situ technique that uses plants and associated soil microbes to degrade, contain, or immobilize pollutants in contaminated media[30]. It can be used for treating a wide range of contaminants such as VOCs, PAHs, PCBs, BTEX and also heavy metals and radionuclides[31,32]. Phytoremediation is probably the most interdisciplinary remediation technique and requires a background in chemistry, biology, ecology, geology and environmental engineering[31].

This technique was developed during the last 30 years, starting from the idea of Chaney, who proposed to use plants to treat soils polluted by heavy metals (Zn, Cr and Cd)[33]; this technique resulted quite effective and immediately got appreciation among the scientific community.

Phytoremediation is generally employed to treat large areas superficially contaminated, where other remediation techniques are not cost effective or practicable; in fact, it has lower installation and maintenance costs (as less as 5%) with respect to other remediation technologies[34]. Current research activities aim to find plants having a fast adsorption kinetics, a high tolerance towards the targeted contaminants and the

ability to degrade or transform the contaminant in inert or, at least, less harmful products.

In summary phytoremediation presents several advantages: it is a cost-effective, environmental-friendly, *in-situ* applicable, and solar-driven (the energy required for the growth is only provided by the sun) remediation technology[32].

Despite the fact that phytoremediation is a promising technique also for the remediation of DNAPLs polluted sites, there are several limitations that should be carefully considered when using it, shortly summarized in figure 3.8[31].

The mechanisms at the basis of phytoremediation include phytoextraction, phytostabilization, rhyzodegradation, phytodegradation (or phytotransformation) and phytovolatilization; the main features of these mechanisms are sketched in Figure. 3.9 and Table 3.3[31,35].

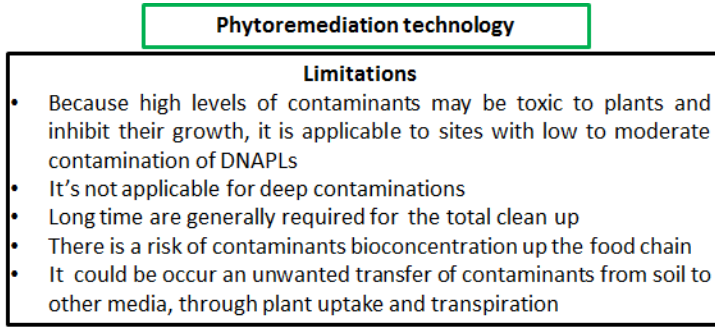

Figure 3.8 Limitations of phytoremediation technology

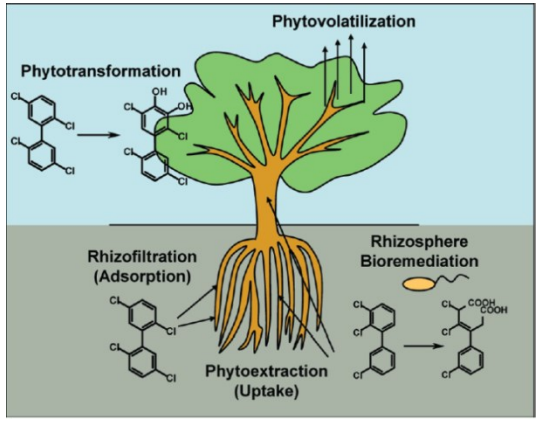

Figure 3.9 Processes involved in phytoremediation of a pollutant

Table 3.3 Summary of the different techniques of phytoremediation

Strategy	Description
Phytoextraction	Accumulation of pollutants in harvestable biomass i.e.,shoots
Phytostabilization	Limiting the mobility and bioavailability of pollutants in soil by plant roots
Rhyzodegradation	Degradation of organic xenobiotics in the rhizosphere by rhizospheric microorganisms
Phytodegradation	Degradation of organic xenobiotics by plant enzymes within plant tissues
Phytovolatilization	Conversion of pollutants to volatile form and their subsequent release to the atmosphere

The uptake mechanism of organic pollutants by plants generally follows the ‘‘Green Liver’’ model proposed by Sandermann (Figure 3.10)[35,36]. The metabolic pathway responsible for the uptake is divided in three step: I)

activation, II) conjugation and III) sequestration.

In the specific case of TCE, the first phase is activated by the oxidation of TCE to trichloroethanol and followed by the conjugation with a plant molecule such as glucose (phase II); finally sequestration of the conjugate compound into the cell wall or within the vacuole occurs (phase III).

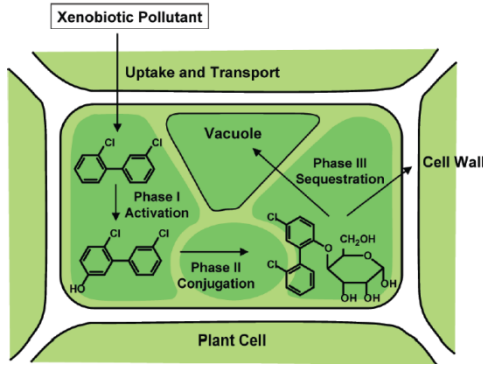

Figure 3.10 The three step of the 'green liver' model

Many studies about phytoremediation are conducted on a laboratory or greenhouse scale and only few researches have been performed to test plants performances in real field conditions[37]. Moreover, the results obtained in field conditions often differ from those at laboratory or greenhouse scale. This is mainly due to the complex interactions of the plants with the environment and temperature, soil moisture, precipitations, nutrients and pH affect in a not predictable way the phytoremediation performance[38].

In the last few years several researches have been addressed

to enhance TCE phytoremediation efficiency[39-43]. In particular, it was shown that transgenic plants such as hybrid poplars, are good candidates for an effective removal of this contaminant from soils[39]. *Populus trichocarpa (black cottonwood) and Populus deltoides* (*eastern cottonwood*), are usually crossed to obtain hybrid species with leaves four times larger than the parental plants[40]; a characteristic that allows to improve the evapotranspiration rate and thus the potential phytoremediation efficiency.

Table 3.4 summarizes the latest works reporting the use of plants for TCE remediation.

Table 3.4 Plants tested for the phytoremediation of TCE polluted site

Plant	[TCE] (mg/L)	Reference
Hybrid poplar	50	44
Hybrid poplar	800	45
Legouminous	50	46
Carrot	0.14-0.56	47
Spinach	0.14-0.56	47
Tomato	0.14-0.56	47
Apple	0.005-0.5	48
Peach	0.005-0.5	48
Transgenic alfaalfa	6-200	49
Willow	144-721	50

In this context, we evaluated the phytoremediation capability of a cultivar of maize to degrade TCE from an artificial polluted medium[51]. Respect to other plants, usually used for phytoremediation studies, *zea mays* presents some advantages briefly resumed in Fig. 3.11[52-54].

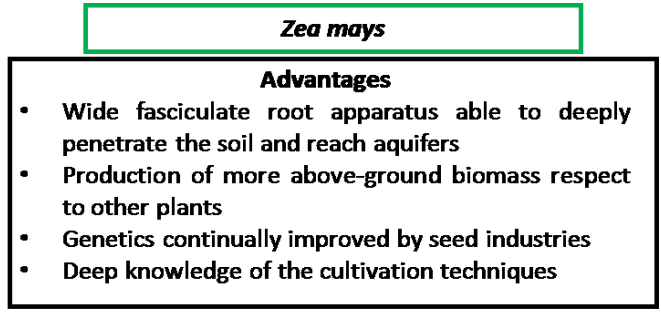

Figure 3.11 Advantages in the use of *zea mays* plant

In this work we demonstrated that *Z. mays* is effective in the removal of TCE from an artificial contaminated soil.

These preliminary results encourage further studies for the employment of *Z. mays* for phytoremediation processes of TCE polluted sites.

3.2.2 Experimental Section

To perform a balance of the TCE used as contaminant, we devised a closed experimental system where we could monitor [TCE] in three different compartments, namely the plant, the growth medium (GM) and the atmosphere.

Figure 3.12 shows a sketch of the experimental bioreactor consisting of a sealed glass jar (Bormioli, V = 1057 mL) where germinated *Z. mays* seeds (Pioneer PT32B10, Monsanto) were exposed to different amounts of TCE (Sigma analytical grade) delivered by sterile glass syringes directly in the growth medium. The atmospheric [TCE] was monitored

by means of a passive sampling apparatus. The passive sampler, RING (Aquaria Research srl), consists of an adsorbent cartridge packed with 300 mg of activated coconut charcoal inserted in a microporous polyethylene membrane. TCE diffuses through the membrane towards the cartridge driven by the gradient of concentration between the ambient air and the inner cartridge. Air TCE concentration (mg/m^3) can be calculated by applying Eq. 2, derived from Fick's first law of diffusion[55,56].

$$[\text{TCE}] = \frac{m_d - m_b}{P \cdot t \cdot 10^6} \qquad (2)$$

where m_d is the adsorbed mass in milligrams of the analyte sampled during the time t (min) while m_b is the mass of the analyte on a non-exposed cartridge, and P (mL/min) is the diffusive uptake rate of the substances (69 mL/min for TCE); P values were supplied by the RING manufacturer. Samplers were exposed at 10 cm above the growth substrate.

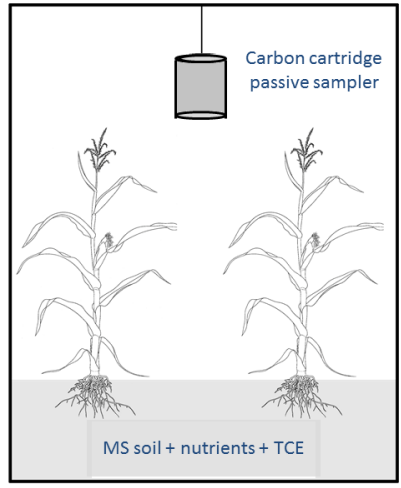

Figure 3.12 Sketch of the experimental bioreactor used for the mass balance assessment

The GM consisted in 4.4 g of a Murashige and Skoog (MS) medium dissolved in 1 L of distilled water containing 8 g of phytoagar (Duchefa- Biochemie, Haarlem, NL) and 30 g of sucrose (Sigma) as carbon source[57].

The *Z. mays* seeds were surface sterilized in axenic conditions by stirring in ethanol (Sigma analytical grade) 70 % for 3 min; successively, they were washed twice with sterile double-distilled water for 1 min, stirred in a 1.5 % sodium hypochlorite (Sigma) solution for 10 min and finally rinsed five times for 1 min with double-distilled sterile water. The seeds were pre-germinated on water sterile imbibed filter paper in Petri dishes; when the rootlet was evident (roughly 3 days), they were sown on solid MS medium in the bioreactor.

Three replicates for each experimental thesis with increasing

TCE amount (58.4, 100, 116.8, 200, 300 mg) were prepared. Given the volume of the bioreactor, the delivered TCE corresponded to a total concentration of contaminant of 55.25, 94.6, 110.5, 189.2 and 283.8 mg/L for each experimental thesis. In each bioreactor, five pre-germinated maize seeds were sown at regular distance on 100 mL of solid GM; in parallel, a series of blank systems was prepared, namely three replicates of bioreactors without plants for each dose of TCE and three replicates of a non-contaminated bioreactor. All the bioreactors were finally placed in a plant growth chamber at 25 ± 1 °C for 9 days (the same temperature was kept both during the day and the night), with a photoperiod of 8 h of dark and 16 h of light ensured by a fluorescence lamp (Mazda TFP 36W JR/865 G13) placed 40 cm from the plants.

To have a better control on the morphometric parameters of the plants, we also prepared a series of glass vials (V = 30 mL) containing the contaminated GM (10 mL) and only one seed. Even in this case, three replicates for each TCE dose were set up.

3.2.3 Products characterization

The three different matrices (air, medium and plants) of each bioreactor were separately analyzed for the detection of TCE and of TCE metabolites by means of GC-MS and LC-MS,

respectively.

After the harvesting, each plant was separated in stem/leaf (aerial part) and roots, weighted, immediately frozen in liquid nitrogen and then stored at −80 °C until use.

Samples were ground to powder in liquid nitrogen to prevent analyte loss. One hundred milligrams of ground sample was treated with 2 mL of 1 M H_2SO_4 /NaCl (10/1 *w*/*w*) (Sigma-Aldrich) solution and then extracted by shaking the sample for 10 min at 6000 rpm with 10 mL of methyl tert-butyl ether (MTBE, Sigma analytical grade)[58]. In the case of metabolite analyses, the samples were extracted with 200 μL of ethyl acetate (Sigma analytical grade) and vortexed for 1 min[58]. In both cases, a small amount of $MgSO_4$ (CARLO ERBA) was added to the mixture to remove the residual water; samples were vortexed for another minute, shaken for further 15 min at 12000 rpm and finally the supernatant was injected into a GC-MS for TCE analysis or LC-MS for metabolite analysis.

In order to check whether any TCE residual was still present in the growth medium at the end of the experiment, the agar was homogenized by mechanical stirring in a sealed vial and three samples of GM (2.8 g, corresponding to a volume of ≈3 cm^3) were extracted by shaking for 10 min at 6000 rpm with 10 mL of MTBE; 1 μL of the supernatant was injected into the GC-MS apparatus. The deviation of the results for the

three different samples was within 5 %.

Passive diffusive samplers were extracted according to the NIOSH methodology[59]. The inner cartridge was desorbed in 2 mL of carbon sulphide (CS_2, Sigma analytical grade) for 30 min, and 1 μL of the supernatant was directly injected in the GC-MS apparatus.

All samples for TCE detection were analyzed by means of a GC-MS apparatus (Agilent Technologies 7890A) by using a DB17MS 30-mt column with an internal diameter of 0.25 mm and with a stationary phase of 0.25 μm thickness. One microliter of each sample was injected in split-less mode; runs lasted 10 min with a flow rate of 0.5 mL/min and with a temperature ramp of 20.5 °C/min up to 240 °C. Calibration curves were built by injecting TCE (Sigma analytical grade) standards at known concentrations prepared in MTBE or CS_2 . The limit of detection (LOD) was estimated from the ratio signal to noise (S/N = 3) and corresponded to 0.15 mg/L in our experimental conditions.

Samples for metabolite analyses were run on a LC-MS apparatus (Waters quattro micro) by direct injection of the sample in the ESI-quadrupole mass detector, both in positive and in negative modes.

3.2.4 Employment of Zea Mays L. in phytoremediation of TCE

To evaluate the absorption capabilities of the *Z. mays* plants towards the TCE added to the GM, we performed a balance of the system, by taking into account that the bioreactor was thermodynamically closed and could not exchange matter with the external environment. Therefore, at the end of the experiments, the initial TCE must be distributed among three different compartments: the plants (1), the GM (2) and the atmosphere (3), either in its initial form or in the form of metabolites eventually produced by the plants. Table 3.5 shows the residual TCE found in the GM (2) and in atmosphere (3), at the end of the experiments for each TCE initial dose.

Table 3.5 Residual TCE found in the GM (2) and in atmosphere (3), at the end of the experiments for each TCE initial dose

TCE_0 (mg)	**58.4**	**100**	**116.8**	**200**	**300**
TCE_2 (μg)	30 ± 2	60 ± 3	< LOD	< LOD	2200 ± 300
TCE_3 (mg)	49 ± 2	82 ± 4	98 ± 3	161 ± 3	235 ± 1
Blank					
TCE_2 (μg)	120 ± 5	160 ± 8	140 ± 3	160 ± 3	2700 ± 400
TCE_3 (mg)	57 ± 1	98 ± 4	114 ± 4	198 ± 3	297 ± 5

Both in the blank systems and in the presence of the plants, TCE was mainly detected in the atmospheric compartment,

and it was found in traces (<0.05 % of TCE_0, except for TCE_0 = 300 mg where $TCE_2 \approx 0.7$ %) in the GM, while it was not detected into the plant tissues, as revealed by GC-MS analyses of the extracted solutions.

We defined a *removal efficiency* (RE, %) of the *Z. mays* as a direct measure of the phytoremediation abilities of the plants. RE was defined in terms of absolute mass (mg) of the removed TCE from the environment (compartments 2 and 3), i.e. the TCE accumulated or metabolized by the plants.

$$RE = \frac{TCE_0 - \sum_i TCE_i}{TCE_0} \times 100 = \left(1 - \frac{\sum_i TCE_i}{TCE_0} \right) \times 100 \quad i = 2,\ 3 \tag{3}$$

TCE_3 mass has been calculated by multiplying $[TCE]_3$ from Eq.2 by the volume of air in the bioreactor ($V_{bioreactor} - V_{GM}$). Figure 3.13a shows the removal efficiency of maize plants for different expositions to the contaminant. In particular, RE is reported as the average of three replicates for each experimental thesis (three sets) containing five seeds for each bioreactor. In all cases, RE was found to be in the range of 15–20 % with the highest efficiency at the higher doses of TCE. RE values take into account a loss of about the 1–3 % of TCE, as revealed by the analyses of the blanks. This was most probably due to the absorption of TCE by the rubber ring

placed underneath the jar caps and used for sealing the bioreactors and/or by a photo-degradation process.

A further indicator of the performances of *Z. mays* is the *specific removal rate* (RR, mg TCE $g^{-1}_{p}\,day^{-1}$) defined as the ratio between the absolute mass (mg) of the removed TCE from the environment and the averaged fresh biomass (g) of *Z. mays* mediated by the total duration of the experiment, *t* (days), for each TCE dose

$$RR = \frac{TCE_0 - \sum_i TCE_i}{t \cdot m_p} \quad i = 2, 3 \qquad (4)$$

where m_P is the total biomass in the bioreactor, as weighted at the end of the experiments; m_P was calculated as the average of the total biomass in each bioreactor at a given TCE amount.

Figure 3.13b shows that the specific removal rate increased with the amount of TCE added in the bioreactor and it reached a value of ~1 mg TCE $g^{-1}_{p}\,day^{-1}$ when plants were exposed to 300 mg of TCE; the same trend was observed when RR was calculated separately with respect to the fresh weight of the roots and of the aerial part (leaves + stems). A comparison with the blank systems revealed that the morphometric data, both in terms of fresh weight (see Table 3.6) and in terms of the length of the roots and the aerial parts

(see Fig. 3.14c, d), is not significantly affected by the addition of TCE in the concentration range 0–300 mg/L.

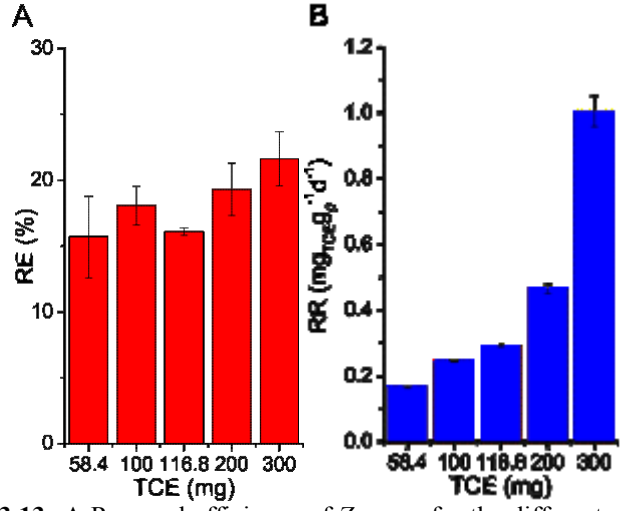

Figure 3.13 **A** Removal efficiency of *Z. mays* for the different amounts of TCE. **B** Removal rate of *Z. mays* for the different amounts of TCE expressed per units of plants fresh weight

To study the effect of the TCE on maize plant morphology, we set up a single seed bioreactor with increasing amount of TCE with respect to the total volume of the bioreactor, namely [TCE] = 667, 1330, 2000 mg/L; TCE concentration was far above those used in the five seed bioreactors, and these experiments only aimed to establish the maize lethal TCE dose, and therefore, RR and RE were not calculated.

Table 3.6 Average fresh biomass and residual TCE at the end of the experiments

TCE_0 (mg)	**TCE removed (mg)**	**Plant biomass (g)**
0	0	7 ± 2

58.4	10 ± 2	6 ± 2
100	18 ± 1	8 ± 2
116.8	19 ± 1	7 ± 2
200	39 ± 3	9 ± 3
300	65 ± 3	7 ± 2

Figure 3.14a gives a clear glimpse of the growth inhibition of the plants caused by increasing amounts of TCE. The picture was taken 3 days after the beginning of the experiments, and it clearly shows how the stems and the roots tended to get thicker and shorter when plants are exposed to higher [TCE], as also highlighted in Fig. 3.14b. Figure 3.14c, d reports the length of the aerial parts (l_a) and of the roots (l_r) of *Z. mays* at the end of experiment.

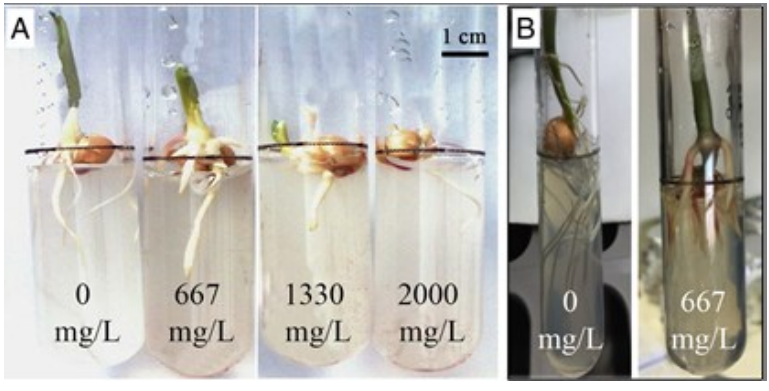

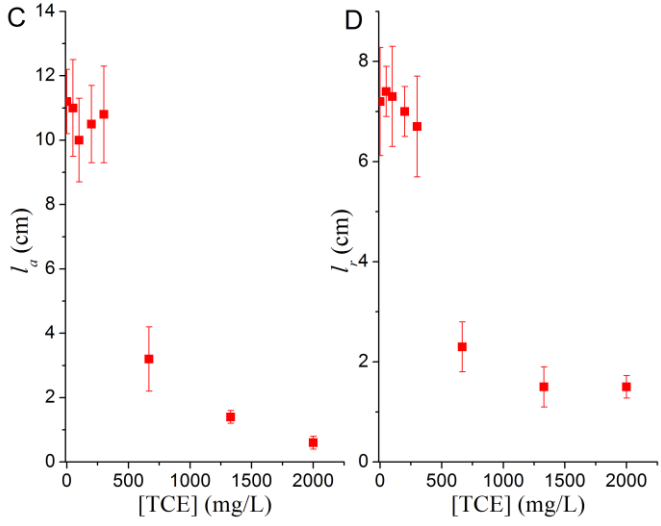

Figure 3.14 **a** Comparison of the effects of TCE on the growth of *Z. mays* plants exposed to increasing concentrations of contaminant. The picture was taken 3 days after the beginning of the experiments. **b** Comparison between the roots of a *blank* system and the roots of a system containing TCE = 667 mg/L. The picture was taken at the end of the experiment. **c, d** Variation of the aerial part (l_a) and root (l_r) lengths of *Z. mays* plants exposed to increasing doses of TCE as measured after 9 days from the beginning of the experiment

Morphometric data suggested that RR could increase with the amount of the contaminant until TCE did not significantly inhibit the plant growth. Therefore, in the investigated concentration range (0–283.8 mg/L), the more TCE was added in the bioreactor, the more *Z. mays* could efficiently remove the contaminant.

To understand the fate of the TCE up taken by maize, we analyzed several samples extracted from the plants by means of the GC-MS apparatus; no traces of the contaminant were

detected neither in the aerial part nor in the roots. A possible explanation to this observation is that *Z. mays* plants were able to completely metabolize the adsorbed TCE during their growth process; therefore, we performed experiments aimed to recognize and characterize metabolites derived from the metabolic modification of the contaminant. Gordon and coworkers investigated the uptake of TCE by different plant species, including poplars and tobacco, and they found a common metabolic pathway for the adsorbed TCE, mainly operated through the cytochrome P450[37,45,60]. The pathway basically followed the 3-step *green liver* model proposed by Sandermann[36]. Trichloroethylene could be initially oxidized to dichloroacetic acid ($CHCl_2COOH$, 128.9 g/mol) or trichloroacetic acid (CCl_3COOH, 163 g/mol) to finally yield oxalic acid ($(COOH)_2$, 90 g/mol), or be oxidized to trichloroethanol ($C_2Cl_3H_2OH$) to finally be conjugated with glucose to yield trichloroethanol glucoside ($C_8H_{13}Cl_3O_6$, 311.5 g/mol); both the oxalic acid and the glucoside then could enter in other biological processes or be excreted by the plants.

To validate this hypothesis, we performed a preliminary screening of samples extracted with ethyl acetate by means of a LC-MS apparatus and we found several TCE metabolites both in root, leaf and stem samples. Fig. 3.15 shows, as an

example, the comparison between the mass spectra of the aerial parts of a blank system with a system containing [TCE] = 110.5 mg/L. Four main metabolites, namely oxalic acid, dichloroacetic acid, trichloroacetic acid and the glucoside, were easily identified through their molecular masses, and the overlapping of the two spectra revealed a higher concentration of these metabolites in the plants exposed to TCE, as shown in the insets of Fig. 3.15. These analyses seem to confirm the metabolic pathway followed by TCE as proposed by Sandermann, even in the case of *Z. mays*, as well as for tobacco and poplars. The absence of any TCE trace in all analyzed plant organs allows to speculate that *Z. mays*, in the TCE concentration range we investigated, is able to metabolize the contaminant.

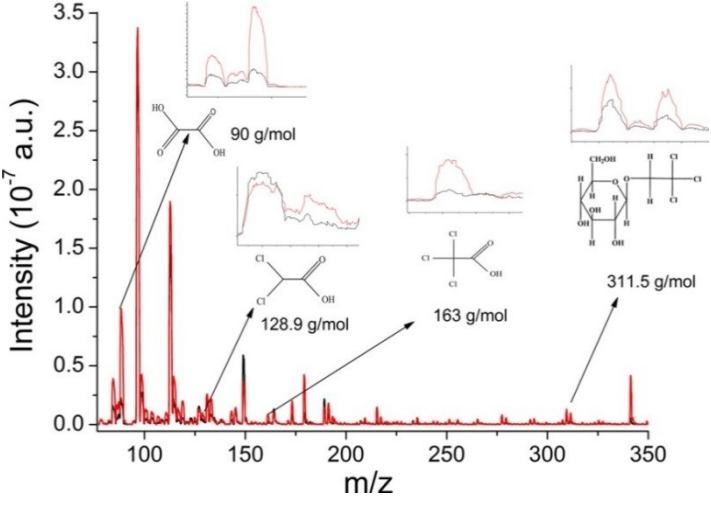

Figure 3.15 Mass spectra of the solutions extracted from the aerial parts of *Z. mays* exposed to 0 mg/L (*black line*) and 110.5 mg/L (*red*

line). *Insets* show the details of the spectra of the different metabolites identified together with their chemical structure and molecular weight

3.2.5 Conclusion

We proved that *Z. mays* is a good candidate for the removal of high TCE amounts from an artificial environment. In particular, we set up a bioreactor where all the compartments (atmosphere, growth medium and plants) could be easily monitored to understand the fate of known amount of trichloroethylene (55–280 mg/L) added to the growth medium, either in the presence or in the absence of *Z. mays* plants. The bioreactor used in our experiments represented an unnatural method of growth and did not reflect the field conditions. However, starting from our results, several improvements can be made to the experimental design to gradually increase the complexity of the system and have a better picture of the plant performances before the use of maize for in situ remediation of TCE. The GC-MS analyses and the accurate TCE balance of the systems revealed that the plants were able to remove and metabolize TCE with an efficiency (RE) ranging from 15 to 20 %, depending on the total amount of the contaminant added to the bioreactor.

A preliminary LC-MS study on the plant extracts revealed the presence of several TCE metabolites, including dichloroacetic and trichloroacetic acids, both in the roots and

in the aerial part of the plants; this suggested that *Z. mays* followed the Sandermann green liver metabolic model.

Our results encourage further studies for the employment of *Z. mays* in phytoremediation processes of soils and waters contaminated by TCE and, potentially, by other chlorinated DNAPLs.

References

(1) ITRC Technical and Regulatory Guidance for Surfactant/Cosolvent Flushing of DNAPL Source Zones, **2003**
(2) Naval Facilities Engineering Command., Design Manual, NFESC Technical Report TR-2206-ENV, **2002**
(3) Rossi F. et al., *Ecol. Model*. **2009**,220,1857–1864
(4) Fendler J.H., *Annu. Rev. Phys. Chem.* **1984**,35,135–157
(5) Mao X. et al., *J. Hazard. Mater.* **2015**,285,419–435
(6) Souza E.C. et al., *Int. Biodeterior. Biodegradation.* **2014**,89,88-94
(7) Svab M. et al., *J. Hazard. Mater.* **2009**,163,410–417
(8) Ranjan R.S. et al., *Environ. Technol*. **2006**,27,767–776
(9) Lee D.H. et al., *Geosci. J.* **2008**,12,63–68
(10) Harendra S. et al., *Ind. Eng. Chem. Res.* **2011**,50, 5831–5837
(11) Albino J.D. et al., *J. Environ. Sci. Health. A*. **2009**,44,1565–1573
(12) Shiau B.J. et al., *Groundwater.* **1994**,32,561–569
(13) Shiau B.J. et al., *Environ. Sci. Technol.* **1995**,30,97–103
(14) Vreysen S. et al., *J. Soils Sediments* **2005**,5,240–244
(15) Rosas J.M. et al., *Chemosphere* **2011**,84,260–264
(16) Intiso A. et al., *Submitted tensioattivi*, **2017**
(17) Canadian Federal Environmental Quality Guidelines Alcohol Ethoxylates, **2013**
(18) Zheng G. et al., *Environ. Sci. Technol.* **2012**,46,12062–12068
(19) Din K. et al., *J. Hazard. Mater.* **2009**,167,575–581
(20) Kalyanasundaram K. et al., *J. Am. Chem. Soc.* **1977**,99,2039–2044
(21) Aguiar J. et al., *J. Colloid Interface Sci*. **2003**,258,116–122
(22) Dominguez A. et al., *J. Chem. Educ.* **1997**,74,1227-1231
(23) Gezae Daful A. et al., *J. Phys. Chem. B.* **2011**,115,3434–3443
(24) Chen C.C. et al., *AIChE J.* **1996**,42,3231–3240
(25) Li X.X. et al., *Fluid Phase Equilibr.* **1998**,153,215–229
(26) Hinz H. J. et al., Springer Science & Business Media, **2012**
(27) Katritzky A.R. et al., *Ind. Eng. Chem. Res.* **2008**,47,9687–9695
(28) Aubery C. et al., *Langmuir.* **2011**,27,14005–14013
(29) Aubery C. et al., *Langmuir.* **2013**,29,1779–1789
(30) Greipsson S., *Phytoremediation. Nat. Educ. Knowl.* **2011**, 2, 7
(31) Hazrat A. et al., *Chemosphere*. **2013**,91,869-881
(32)U.S.EPA document, https://clu-in.org/download/remed/542f06013.pdf
(33) Chaney R.L., Noyes Data Corp., Park Ridge, NJ, **1983**,50–76
(34) Van Aken B., *Curr. Opin. Biotechnol*. **2009**,20,231–236.
(35) Van Aken B. et al., *Environ. Sci. Technol.* **2010**,44,2767–2776
(36) Sandermann H., *Pharmacogenetics.* **1994**,4,225–241
(37) Shang T.Q. et al., *Phytochemistry.* **2001**,58,1055–1065
(38) Vangronsveld J. et al., *Environ. Sci. Pollut. Res.* **2009**,16, 765-794

(39) Van Aken B., *Trends Biotechnol.* **2008**,26,225-227
(40) Chappell J., U.S.EPA document , **1997**
(41) Newman L.A. et al., *J. Soil. Contamin.* **1998**, 7,531–542
(42) Gerhardt K.E. et al., *Plant Sci.* **2009**,176,20–30
(43) Cruz M.D. et al., *Environ. Sci. Pollut. Res.* **2014**,21,13.909–13.928
(44) Gordon M. et al, *Environ. Health. Perspect.* **1998**,106,1001–1004
(45) Newman L.A. et al., *Environ. Sci. Technol.* **1997**,31,1062–1067
(46) Doty S.L. et al., *Water Res.* **2003**,37,441–449
(47) Schnabel W.E. et al., *Water Res.* **1997**,31,816–824
(48) Chard B.K. et al., *Environ. Sci. Technol.* **2006**,40,4788–4793
(49) Zhang Y. et al., *J. Hazard. Mater.* **2013**,260,1100–1107
(50) Schoftner P. et al., *Int. J. Phytoremed.* **2016**,18,686-692
(51) Moccia E. et al., *Environ. Sci. Pollut. Res.* **2017**,24,11053-11060
(52) Vamerali T. et al., *Environ. Chem. Lett.* **2010**,8,1–17
(53) Wuana R.A. et al., *African J. Gen. Agri.* **2010**,6,275–287
(54) Baldantoni D. et al., Nova Science Publisher Inc., **2011**,631–649
(55) Cussler E.L., Cambridge University Press, **2009**
(56) Rossi F. et al., *Aiche J.* **2015**,61,3511-3515
(57) Murashige T. et al., *Physiol. Plant.* **1962**,15,473–497
(58) Odom L. et al., *J. Environ. Eng.* **2013**,139,1162–1167
(59) NIOSH manual of analytical methods
http://www.cdc.gov/niosh/docs/ 2003-154/ **2003**
(60) Doty S.L. et al., *Proc. Nat. Acad. Sci.* **2007**,104,816-821

CHAPTER IV: Catalytic oxidation of trichloroethylene

4.1 Introduction

VOCs are emitted from a wide range of outdoor and indoor sources, such as transport and industrial process as well as from household products[1,2]. These compounds have been identified as components of the photochemical smog and responsible for ground-level smog formation, tropospheric ozone formation, stratospheric ozone depletion and climate change[3]. Among VOCs, Cl-VOCs are organochlorines compounds that present widespread applications in industry and show high toxicity and stability in the environment[4].

Several techniques have been developed for the destruction of these contaminants from gases[5,6]. For many years, thermal incineration was the most common process to obtain the total combustion of highly concentrated Cl-VOCs[7]. Despite of several advantages, this technique suffers some limitations such as high energy consumption for the combustion process and the production of undesirable byproducts (e.g., NO_x, dioxins and carbon monoxide)[8].

Catalytic oxidation represents an effective and economically alternative for the oxidation of Cl-VOCs into CO_2, water, and other less harmful products[9]. Catalysts allow to work at much lower temperatures (250-500 °C) than thermal

incineration process, which results in two mainly advantages: lower energetic and operative costs, and reduction of undesirable byproducts formation.

Generally, catalytic activity is evaluated by monitoring the conversion as function of the temperature (also known as light-off curve)[5]. T_{50} and T_{90} (temperatures at which 50 % and 90 % conversion are reached) are commonly used to evaluate catalyst activity.

Catalyst activity, selectivity and stability are fundamental parameters to address the choice of an efficient material for the abatement of Cl-VOCs. Several factors such as water and other VOCs as hydrogen-supplying compounds, can influence catalytic activity and product selectivity[5].

Catalyst deactivation is due to several mechanisms that occur depending on the type of the reaction. The most important are: coke deposition, poisoning, volatilization of active phase, and thermal degradation[5].

4.2 Catalysts for VOCs elimination

Historically, catalysts used for the oxidation of VOCs can be classified into two major groups: noble metals and transition metal oxides[5].

Supported noble metals (Pt, Pd, Au, Ag, Rh etc.) are commonly used due to their high efficiency at low

temperatures[9]. The most used catalyst supports are metallic material (aluminum or stainless steel) or ceramics (cordierite) in monolithic or honeycomb form.

The catalytic performance depends on the noble metal, preparation method, metal loading, precursor type, particle size and finally the nature of VOC. Table 4.1 summarizes the performance of different noble metal catalysts recently reported.

Table 4.1 Noble-metal catalysts for the oxidation of VOCs

Catalyst	**Support**	**VOCs**	**T_{50} (°C)**	**T_{90} (°C)**	**Reference**
Pt	Al_2O_3	DCE	288	350	(10)
Pt	Al_2O_3	PCE	577	660	(10)
Pt	Activated carbon	Benzene	105	110	(11)
Pt	H-beta	TCE	380	460	(12)
Pd	Al_2O_3	DCE	362	416	(10)
Pd	Al_2O_3	PCE	539	632	(10)
Pd	H-beta	TCE	310	380	(12)
Pd	Co_3O_4	Xilene	232	249	(13)
Au	Fe_2O_3	Toluene	200	260	(14)
Au	CeO_2-ZrO_2-TiO_2	Propane	360	420	(15)

Noble metal based catalysts present some disadvantages such as high cost, deactivation by sintering or poisoning and a low selectivity when employed alone (bulk material without any dispersion on a support).

Non-noble metal oxide catalysts are considered as low cost alternatives for the removal of VOCs from gases[5]. The most common metals employed for this purpose are Ce, Co, Cu, Ti, V, Mn, Fe, Ni, Nb, Zr, Mo and Cr[6]. Figure 4.1 summarizes the advantages of non-noble metal oxide catalysts. However, catalytic activity of these materials is generally not as good as that of the noble metal based catalysts[7]. In order to achieve a comparable performance to noble metals, a combination of two or more oxides is usually used.

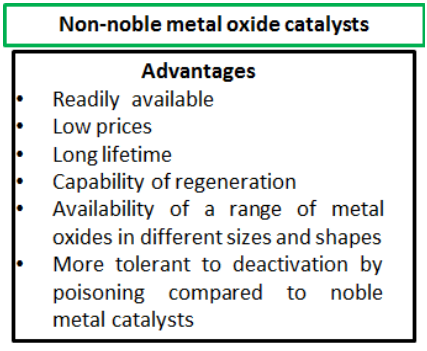

Figure 4.1 Advantages of non-noble metal oxide catalysts

Generally, non-noble metal oxide catalysts can be prepared as bulk materials or deposited on a support; the latter showed better performances than unsupported materials thanks to a greater dispersion of the active component.

Preparation method and support material are fundamental to address the activity of non-noble metal oxide catalysts.

In the literature there are several studies reporting different

preparation methods in order to obtain porous supports. These kind of materials generally present high surface and large pores which promote a higher dispersion and enhance catalytic performance in the oxidation of VOCs.

Table 4.2 reports some examples of non-noble metal catalysts for the abatement of VOCs.

Table 4.2 Non-noble-metal catalysts for the oxidation of VOCs

Catalyst	Support	VOCs	T_{50} (°C)	T_{90} (°C)	Reference
CeO_2	/	DCE	320	390	(16)
CeO_2	/	TCE	425	490	(16)
$Ce_{0.5}Zr_{0.5}O_2$	/	DCE	295	395	(16)
Co_3O_4	Clay	EDC	290	345	(17)
Co_3O_4	Clay	Acetylene	280	310	(18)
Co_3O_4	/	Propylene	310	350	(18)
CuO	H-beta	TCE	310	375	(19)
Cu/Co oxide	/	Benzene	255	290	(20)

As described above, the properties of the support (hydrophobicity, acidity, pore structure, and redox properties), have a significant influence on the oxidation of VOCs.

In the last few years several catalysts have been studied for the catalytic oxidation of TCE[21-26].

Metal oxides and supported noble metals have been successfully used, but they present problems related with the

catalyst deactivation and with the formation of toxic by-products, such as Cl_2 and PCE[27].

Blanch-Raga et al. prepared and used hydrotalcite-like compounds to host metal catalysts, such as Mg(Fe/Al), Ni(Fe/Al)and Co(Fe/Al), showing good performances for the TCE oxidation, mainly due to the presence of $O_2^-$and O_2^{2-} sites that enhance the catalytic productivity[28]. At the same time, the authors observed the formation of several by-products (HCl, PCE and Cl_2).

Acid zeolites have been also tested as alternative catalysts for the TCE oxidation. These materials showed a good activity but suffer a deactivation process due to coke deposition and chlorine attack to the acid sites[29].

A combination of transition metals and zeolites was also exploited in order to improve the catalyst activity and the reaction selectivity towards not harmful products. Divakar et al. studied the catalytic activity of beta zeolites and ZSM-5 with Fe[30]. It was found that all the catalysts were active for the TCE oxidation, but the obtained results depend on the catalyst preparation method.

In this way, Blanch-Raga et al. used copper and cobalt beta zeolites; once again they found that the preparation method has a significant role on the catalytic properties of the materials[19]. Cu-beta prepared by ion exchange was found the

best catalyst in terms of performance and selectivity of the reaction. Moreover no catalyst deactivation after 70 hours of reaction was observed.

Several studies are directed toward new synthetic routes in order to prepare catalysts able to oxidize TCE with high performance, selectivity and stability.

In this context we have successfully employed mayenite ($Ca_{12}Al_{14}O_{33}$) as active catalyst in the TCE oxidation reaction[31]. More details about this material and its application will be discussed in the next paragraphs.

4.3 Use of mayenite as active support in catalysis

Mayenite, labeled as C12A7, is a mesoporous calcium aluminate ($12CaO{\cdot}7Al_2O_3$) which has a positively charged lattice framework $[Ca_{24}Al_{28}O_{64}]^{4+}$ per unit cell that includes two molecules and twelve cages with a free space of 0.4 nm in diameter[31]. The chemical formula for the unit cell may be represented as $[Ca_{24}Al_{28}O_{64}]^{4+}\cdot 2O^{2-}$ and it has a body centered cubic crystal structure belonging to the *I*-43*d* space group with a = 11.989 Å and Z =2 (fig. 4.2).

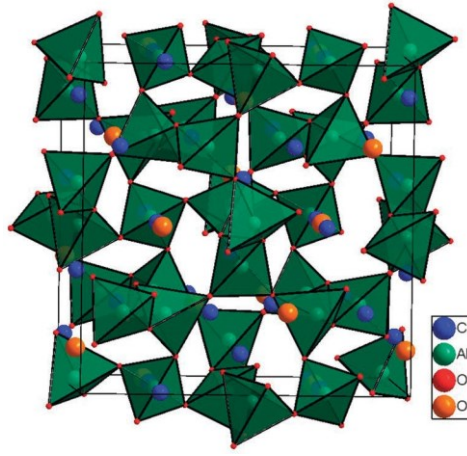

Figure 4.2 Unit cell of mayenite. The "free oxygen" ions are marked as O*

The two oxide ions O^{2-}, namely "free oxygen", are trapped in the cages defined by the framework satisfying the overall electroneutrality condition. Due to the space confinement, the guest species are limited to mono or diatomics such as O^{2-}, O^{-}, O_2^{-}, O_2^{2-}, OH^{-} [32,33]. Mayenite derivatives were obtained by exchanging the O^{2-} anions with other active species, such as OH^{-}, F^{-} and Cl^{-}, O_2^{-} and H^{-} [34-42].

Several studies have been also developed to evaluate the influence of cationic substitutions on this material[43,44]. In particular Ca^{2+} can be partially replaced by Cu^{2+}, Fe^{2+} and Mg^{2+}.

Recently, ionic conducing ceramics have received increasing interest as active catalyst supports[45]. Furthermore, the ability of storing oxygen ions in the nanocages is a unique properties

of mayenite and several works show its application in catalytic process as oxidant species[45]. The most promising characteristic of mayenite to be exploited for catalysis is that the encaged oxygen species can migrate between the surface and the bulk. They can be gradually released at elevated temperatures or stored[46-48]. Therefore, the reported catalytic activity properties of mayenite have often been associated with its strong oxidation ability.

Indeed, the use of mayenite as substrate for Ni catalyst was reported for biomass tar steam reforming in a fixed bed reactor using toluene as tar destruction model compound. 1% Ni on mayenite shows excellent performances either in absence and presence of H_2S. Moreover, $Ni/Ca_{12}Al_{14}O_{33}$ showed excellent sustainability against coke formation due to the "free oxygen" in the catalyst. O_2^{2-} and O_2^- inhibit Ni poisoning by sulphur incorporation in the cages[49].

Hosono et al. have investigated the partial oxidation of methane to CO and H_2 over mayenite promoted metals such as Ni, Co, Pt, Rh and Ru[50]. On Ni, Pt and Pd/C12A7, this reaction readily happened at temperatures as low as 500°C and attained thermodynamic equilibrium. Mayenite without any metal catalyst shows at the same time good performance in the partial oxidation of methane. Furthermore, ethane and ethene were also formed at temperatures higher than 650°C

(10% selectivity at 800°C) due to the existence of active oxygen (O^-, O^{2-}, O_2^{2-}) in C12A7 which readily activated methane into radicals and caused their coupling. When mayenite was promoted by Ni, Pt and Pd, partial oxidation of methane into CO and H_2 readily proceeded even at 500°C.

In 2008, Ruszak et al. studied the high temperature decomposition of nitrous oxide, N_2O, over mayenite[51].

This application is very interesting because in the nitric acid plants, N_2O is an indesiderable by-product and two types of deN_2O technologies are available on market: a non-catalytic and a catalytic one. The non-catalytic technique involves the thermal destruction of N_2O and mayenite support can be used in this context. Authors show an appreciable conversion of N_2O above 850K and upon reaching the process temperature of 1150K the decomposition of nitrous oxide achieved ca. 90%. From a mechanicistic point of view, for the N_2O decomposition over oxide catalysts not containing transition metal ions the anionic redox mechanism initiated by the oxygen atom transfer was proposed. In this context the peculiar feature of mayenite, with its large capacity for storage of the subsurface oxygen species, opens two interesting mechanistic pathways. They consist in suprafacial recombination of surface peroxy ions and intrafacial recombination of surface peroxy with cage and surface

oxygen species as also shown in figure 4.3:

$$O_2^{2-}{}_{(surf)} + O_2^{\ x-}{}_{(cage)} \longrightarrow O_2 + O^{2-}{}_{(surf)} + O^{x-}{}_{(cage)}$$

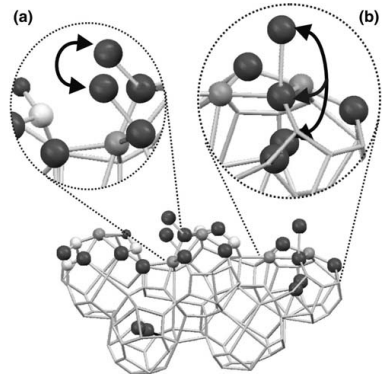

Figure 4.3 Suprafacial (a) and intrafacial (b) recombination of oxygen atoms produced upon dissociation of N_2O

The ability of mayenite as active catalyst for the VOCs oxidation was investigated by Fujita et al.[52]. They synthesized and tested different calcium aluminosilicate, $Ca_{12}Al_{14}O_{33}$, $Ca_{12}Al_{14}Si_2O_{34}$ (C12A6), and $Ca_{12}Al_{10}Si_4O_{35}$ (C12A5) respectively for the total oxidation of propylene and benzene.

Mayenite was found the most active catalyst for the oxidation of both pollutants. Moreover, different amounts of superoxide (O_2^-) and peroxide (O_2^{2-}) anions occluded in the lattice of the calcium aluminosilicates were discovered. Nevertheless, no activity improvement was observed for the oxidation of

propylene and benzene by increasing the amounts of O^{2-} and O_2^{2-}.

In this context we have recently reported the use of mayenite as active catalyst in the TCE oxidation reaction[31,53]. The results showed that TCE was totally converted in CO_2 and CO and the released chlorine was incorporated in the mayenite structure. The high performance of the catalyst could be connected to its oxidative properties due to the presence of $O^{2-}$and O_2^{2-} anions sites that favour the total oxidation of TCE and avoid the formation of coke.

Then we investigated how metal loading can improve mayenite activity[54]. The results showed that Fe doped mayenite promoted the oxidation of TCE in the temperature range 250-450° C. Therefore, the enhanced activity of the catalyst was associated to the presence of the metal, that can reduce the temperature requested for the total conversion of the pollutant.

Starting from these results, I continued my research thanks to an Erasmus traineeship project, spending six months at the ITQ-UPV. Here, I prepared and characterized mayenite catalyst by different method, namely hydrothermal, sol-gel and ceramic, to tune the physicochemical properties (crystalline structure, surface area, redox properties) of the material and evaluate the influence of preparation route on the

catalyst activity for the TCE oxidation[55]. Mayenite prepared by hydrothermal route was found the best catalyst synthesized in the TCE oxidation reaction. From the characterization results it was possible to conclude that mayenite prepared by the hydrothermal method has a good combination of surface area and redox properties that explain the great activity of this material. Moreover the effect of water vapour on the TCE catalytic oxidation was also investigated. The results showed that the addition of water to the feed stream did not alter the activity of these materials. Furthermore stability test exhibited that after five hours of reaction a relevant deactivation of hydrothermal mayenite occurred.

Finally, in order to improve the surface area of the catalyst, we developed a new fast and simple method to prepare mayenite, using PMMA as a soft template agent[56,57].

Mayenite prepared adding 10% w/w of PMMA, showed better performances respect to all previous mayenite synthesized.

The high surface area and the relevant number of superoxide anions (O_2^-) of the mayenite seem to be the main properties determining the best catalytic activity observed.

4.4 Mayenites catalysts preparation

Mayenite based catalyst was prepared by following the ceramic method proposed by Li et al., as follows: a stoichiometric mixture of $Ca(OH)_2$ and $Al(OH)_3$, 41.5 and 50.7 g respectively, was added to 1 L of distilled water[58]. The mixture was grounded under magnetic stirring for 4 h at room temperature, afterwards, was placed in stainless steel autoclave at 150 °C for 5 h. The obtained solid was filtrated and dried at 120 °C overnight, crushed into fine powder and finally placed into a furnace at 1000 °C in air for 4 hours.

Mayenite loaded with different amount of iron (1.5 and 2.0 %) was prepared by adding the calcium aluminium oxide, to a solution containing the desired amount of $Fe(acac)_3$ dissolved in 0.5 L of toluene[59]. The slurry was stirred for 2 days at RT and then toluene was removed with a rotary evaporator. The solid was recovered, dried under vacuum at 50°C for one night and calcined at 1000°C in air atmosphere for 4 hours.

Mayenites tested during the visiting period at the ITQ were prepared as follow: hydrothermal and ceramic mayenite were synthesized by following the procedure described by Li et al.[58]. For the hydrothermal method a stoichiometric mixture of $Ca(OH)_2$ and $Al(OH)_3$ was added to 1 L of distilled water. The mixture was grounded to powder under magnetic stirring for 4 h at room temperature, afterwards, was placed in a

stainless-steel autoclave at 150 °C for 5 h. The recovered solid was filtrated and dried at 120 °C for 8h, crushed into fine powder and finally placed into a furnace at 600 °C in air atmosphere for 4 hours. Ceramic mayenite was synthesized following the same procedure described above[58].

Sol-gel mayenite was prepared according to the method proposed by Ude et al., as follows: 69.6 g of calcium nitrate tetrahydrate, $Ca(NO_3)_2 \cdot 4H_2O$, and 111.6 g of $Al(NO_3)_3 \cdot 9H_2O$ were dissolved in 1.5 L of distilled water[60]. The mixture was heated at 60 °C, then 5 g of citric acid, $C_6H_8O_7$, were added. The citrate-nitrate mixture was heated and vigorously stirred at 90 °C until a gel was formed (about 12 h). The resulting gel was placed in a drying oven at 120 ° C until a cake-like structure was produced. The solid was then crushed into fine powder and finally calcined at 1000 °C in air atmosphere for 4 h.

PMMA mayenites were prepared by adding different amount of polymer (10, 20 % w/w) to a stoichiometric mixture of $Ca(OH)_2$ and $Al(OH)_3$ stirred in 1L of distilled water. The mixture was grounded to powder under magnetic stirring for 4 h, then, placed in a teflon-lined stainless-steel autoclave at 150 °C for 5 h. The solid was recovered by filtration and dried at 120°C for 8 hours. After, the solid was calcined as follows: 1) 2.6 °C/min from RT up to 500°C in N_2 atmosphere; 2)

500°C for 4 hours in N_2; in order to eliminate PMMA template from mayenite precursor 3) 1.7 °C min from 500 to 600 °C in air atmosphere and finally 4) 600 °C in air for 4 hours to obtain the mayenite phase.

All synthesized catalysts were pelletized, and then the pellets were crushed and sieved to obtain grains of 0.2–0.4 mm in diameter. Materials were named as Maye Y, where Y corresponds to the preparation method of the catalyst, i.e. HA (hydrothermal), SG (sol-gel) and CR (ceramic); in case of PMMA mayenites corresponds to the amount of PMMA added in the synthesis, i.e. 10 (10 % w/w of PMMA) and 20 (20 % w/w of PMMA).

4.5 Catalysts characterization

X-ray diffraction patterns were obtained on a Bruker D8 Advance automatic diffractometer operating with a nickel-filtered CuKα radiation. Data were recorded in the 2θ range of 4-80° with the resolution of 0.02°.

The BET surface area of the catalyst were determined using a Nova Quantachrome 4200e instrument using nitrogen as the probe molecule at liquid nitrogen temperature (-196°C). Before the adsorption measurement, mayenite sample was degassed at 200°C under vacuum for 12 h. The surface area values were determined by using 11-point BET analysis.

Particle sizing experiments were carried out by means of laser diffractometer, using an Mastersizer 2000 instrument (Malvern Instrument ltd) operating at 25°C.

Iron content in Fe/Mayenite catalaysts was determined by ICP-OES analysis by digesting the sample in HNO_3. Three replicates for each sample were prepared and the metal loading were calculated by comparison with a calibration curve.

Temperature programmed reduction (TPR) experiments were performed using a TPD-TPR Autochem 2910 analyzer equipped with a thermal conductivity detector. Samples (10-20 mg) were reduced from 25 to 800 °C with a thermal ramp of 10 °C min^{-1} using a N_2:H_2 flow (10% H_2) of 50 mL min^{-1}.

The morphological analysis was investigated using a field emission scanning electron microscopy (FE-SEM) (Zeiss Ultra 55), and the elemental analysis was carried out with energy-dispersive X-ray spectroscopy (EDX) (INCA, Oxford).

The Raman spectroscopy experiments were carried out using a Horiba Jobin Yvon–Labram HR UV–visible–NIR Raman Spectrometer, using a 514 nm wavelength laser for excitation. The spectra were recorded averaging 10 scans obtained in different points of the sample at a resolution of 2 cm^{-1}.

TGA measurements were performed using a thermogravimetric analyzer (TA instruments, TGA Q500) on 5 mg samples, over a temperature range from 25 to 900°C , at a heating rate of 10 °C/min, under an inert atmosphere of nitrogen.

4.6 Experimental Section

4.6.1 Italian experimental set-up

Experiments were carried out at atmospheric pressure in a stainless-steel fixed bed reactor (150 mm long, 22 mm o.d, 18 mm i.d) schematically shown in Fig. 4.4.

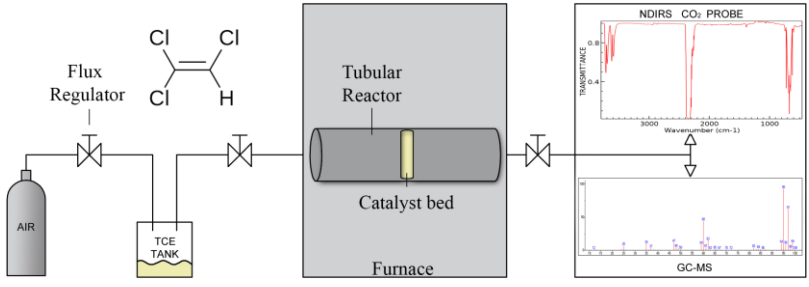

Figure 4.4 Sketch of the experimental setup

The catalytic bed (0.8 g of mayenite) was placed into the reactor between two quartz fiberglass layers. The reactor was placed in an electrically-heated furnace, and the temperature was measured by a K-thermocouple. Catalytic oxidation reactions were carried out at different temperature, between

150°C and 550 °C for 0.09 h. Mayenite was conditioned at the operative temperature with air for 30 minutes prior the TCE injections. The gaseous mixture, composed by trichloroethylene (1700 ppm) and wet air (RH=60 %), was introduced into the reactor at 110 mL/min (Gas Hourly Space Velocity**,** GHSV = 6000 h^{-1}). The gaseous mixture was prepared by sparging with air a vessel containing 1 μL of pure TCE. Blank experiments were made in the same conditions without the presence of the catalyst for all the investigated temperatures.

Gaseous reaction products were collected in a Tedlar sampling bag (SKC, Inc., USA) before analyses. TCE and VOCs concentrations were determined by gas chromatography by using a GC-MS (Agilent 7890A) equipped with a DB 17-MS column (30 m x 0.25 mm 250 μm). A GC oven was run isothermally at 100 °C for 10 minutes. Helium was used as carrier gas with a flow rate of 0.5 mL/min and 1.0 mL of sample was analyzed in a split-less injection mode. NDIRS on line probe (Q-Track Plus IAQ Monitor, TSI) was coupled to the reactor to monitor the concentration of CO_2 and CO resulting from TCE oxidation and the relative humidity (RH %)[61]. Molecular chlorine, Cl_2 (m/z= 71), was determined by SIM mode GC-MS analysis, using the same operative conditions described for VOCs

analysis[62]. Moreover, the production of Cl_2 was also checked by means of iodometric titration, by bubbling the effluent stream through a 0.06 M solution of KI and 0.1 M of H_2SO_4 using soluble starch as indicator.

Cl^- ions were determined by bubbling the effluent into a 2.6/0.76 mM solution of $NaHCO_3/Na_2CO_3$ and analyzing the resulting chloride amount through ion chromatography (IC) using a Dionex DX 120 (Dionex, Sunnyvale, CA, USA) equipped with a Ion Pac AS14 column (4 mm x 250 mm). Moreover 0.5 g of catalyst were extracted with 3 mL of 2.6/0.76 mM solution of $NaHCO_3/Na_2CO_3$ and analyzed by means of IC with the same experimental conditions used for the gas.

The conversion yield of TCE was defined as the ratio between the reacted TCE over the total TCE delivered into the reactor and it can be calculated by means of equation (1)

$$\text{TCE conversion}\left[\%\right] = \frac{m^{i}_{TCE} - m^{o}_{TCE}}{m^{i}_{TCE}} \times 100 \qquad (1)$$

where m^{i}_{TCE} are the moles of TCE delivered into the reactor and m^{o}_{TCE} are the number of moles measured at the reactor outlet.

4.6.2 Spanish experimental set-up

Catalytic experiments have been carried out in a quartz fixed bed reactor. The catalytic bed (0.7 g) was placed on a quartz plug located in the middle of the reactor. Silicon carbide (>0.6 μm) was introduced above the catalyst as a preheating zone. The temperature was controlled using a K-thermocouple located in the middle of the reactor and the reactor was heated using an electrical furnace[19]. The flow rate, composed by dry synthetic air and trichloroethylene (1000 ppm), was set at 400 mL/min (Gas Hourly Space Velocity, GHSV = 12.000 h^{-1}).

A constant trichloroethylene concentration in the inlet gases was assured, by evaporating with air a vessel containing pure TCE held at a controlled temperature (0 °C).

Based on the packing volume of the catalyst, the residence time calculated was 0.24 s. Catalytic tests have been performed by increasing the temperature from 150 to 550 °C in steps of 50 °C. Each temperature was kept 30 min before the analysis of the outlet gases and the total length of the experiment was about six hours.

The outlet gases were analyzed by using a Varian 3630 gas chromatograph system equipped with two columns/detectors[28].

Residual TCE and the organic compounds of the gas flow were separated with a HP-5 column and quantified with a

flame ionization detector. CO_x species (CO and CO_2) were separated with micro-packed columns and analyzed with a thermal conductivity detector. Furthermore, a solution of sodium hydroxide ([NaOH] = 0.0125 M) was used to adsorb chlorine species (Cl_2 and HCl) contained in the outlet gases. Absorbed Cl_2 was quantified by titration and the HCl concentration was measured using a chloride ion selective electrode.

All experiments were repeated three times to ensure the reproducibility of the results. In all the tests the error analysis of triplicate results was below 5%.

4.7 Results and discussion

4.7.1 Mayenite and Fe_2O_3-Mayenite catalysts for TCE oxidation reaction (Italy)

The crystalline structure of the synthesized catalysts were investigated by means of X-ray diffractometry and the spectra are reported in Fig. 4.5. Mayenite structure was indexed within I-43d group. The mayenite XRD pattern presents the characteristic peaks of mayenite around 2θ = 18.1°, 30°, 33.4°, 36.7°, 41.2°, 46.7°, 55.2° and 57.4°. $Ca_3Al_2O_6$ (●) and $CaAl_2O_4$ (**Δ**) were also detected in trace as usual impurities formed during the mayenite preparation processes[46].

Moreover, no peaks associated to the presence of iron species

were observed for 2.0% Fe/Mayenite catalyst. This absence of signal may be due to the low metal loading in the mayenite structure.

Mayenite sample showed a particle sizing of 70 μm. BET surface area and ICP results for synthesized catalysts are summarized in Table 4.3.

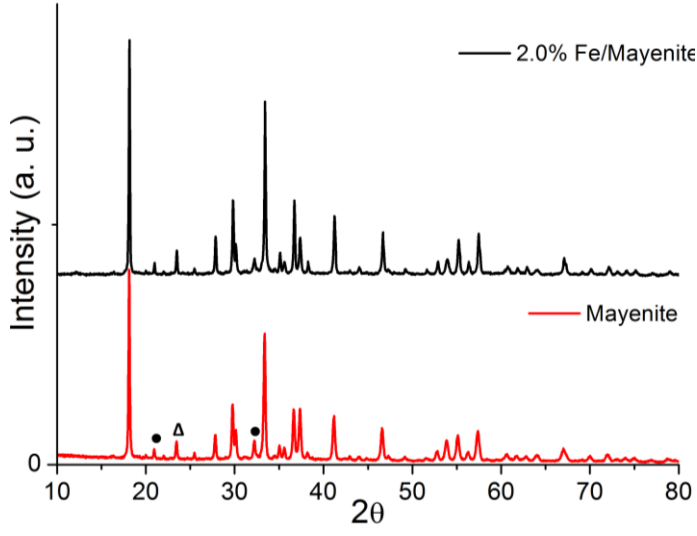

Figure 4.5 XRD patterns of Mayenite (red) and 2.0% Fe/Mayenite (black) catalyst

Table 4.3 Physicochemical properties for the fresh catalysts

Catalyst	Fe content (wt.%)	BET surface area (m^2/g)
Mayenite	-	11.7
1.5 % Fe/Mayenite	1.72	11.5
2.0 % Fe/Mayenite	2.30	11.2

ICP analysis confirmed that metal loading on catalyst structure was close to the nominal value. Mayenite surface area was 11.7 m^2/g, in accordance with those reported for this type of material[40]. All Fe/mayenite samples showed a lower surface area compared to pure mayenite, indicating that Fe particles added to mayenite structure blocked some pores, slightly reducing the access to the internal surface of these materials.

All prepared catalysts have been tested for the oxidation of TCE by evaluating the % TCE conversion (Eq. 1) as function of the temperature.

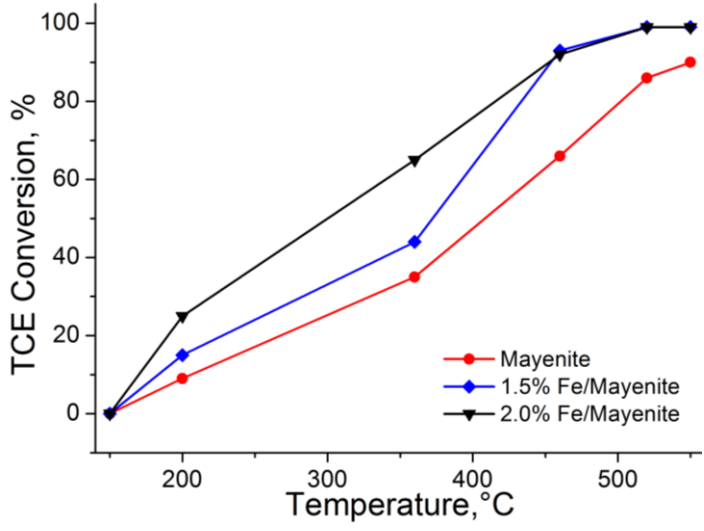

Figure 4.6 TCE conversion for Mayenite (red), 1.5% (blue) and 2.0% (black) Fe/Mayenites

Figure 4.6 shows the comparison of the TCE conversion curve among the synthesized catalysts.

Concerning mayenite catalyst, for low temperatures (< 300 °C) we could not observe a significant degradation of the chlorinated compound and the concentration of TCE at the reactor outlet was found the same as at the reactor inlet.

The catalytic oxidation of trichloroethylene started at 300 °C where 25% of the delivered TCE was converted. The conversion yield was found to increase drastically with the temperature, and it passed from 25% to 65% and 90% for a temperature of 460 °C and 550 °C, respectively. As mentioned in the previous paragraph, the free oxygen present in the mayenite framework were the active species responsible for the TCE degradation. This is consistent with the temperature dependence of the conversion yield; in fact, as reported in previous works, mayenite, at higher temperatures, interacts with the atmospheric O_2 to form reactive oxygen species (O^{2-}, O^-, O_2^-) that, in turn, can react and oxidize TCE to CO_2 and CO[47].

As it can be seen from Figure 4.6, mayenite loaded with the maximum amount of Fe (2.0 %) was found the best catalyst synthesized for the TCE oxidation reaction. This result was related to the strong interaction between the transition metal with mayenite framework, that enhanced the catalytic performance of the material[25].

Blank experiments, performed without using catalyst at any investigated temperatures, have shown no significant results in terms of TCE conversion.

In order to understand the reaction mechanism and to characterize the distribution products, GC-MS analyses were performed in full-spectrum mode to detect the presence of other organic compounds. Moreover a NDIRS technique was used to monitor the presence of CO_x species. Both the chromatographic and the IR analyses showed that for all the catalysts tested, CO_2 and CO were the main carbon products, with a 50:50 percentage of selectivity.

The analyses of chlorinated derivatives of TCE were performed by means of ionic chromatography and iodometric titration. In particular, we were interested in finding chlorine-derivatives in the form of molecular chlorine, Cl_2, chloride ions, Cl^-, or chlorine-oxo species, ClO_x, as generally resulting from the TCE decomposition[19,28]. Iodometric titration did not reveal the presence of Cl_2 and this result was also confirmed by GC-MS analysis in SIM mode, centered on the mass m/z = 70 ± 1. To find Cl^- and ClO_x both the gases at the exit of the reactor and the catalytic material were analyzed. Gases were bubbled in an aqueous solution of $NaHCO_3/Na_2CO_3$ and 20 μL of the solution were injected in an ionic chromatograph equipped with a negatively charged column for anion

detection. The same procedure was applied for the analysis of the used catalysts, which were extracted with the carbonate buffer. IC revealed that Cl^- ions were present only on the catalytic material and no other chlorinated species were detected in the gases or in the mayenite. This result is consistent with the fact that mayenite tends to adsorb Cl^- to form chloro-mayenite (Brearleyite, $Ca_{12}Al_{14}O_{32}Cl_2$) due to the substitution of free oxygen molecules with chlorides[41].

These results were also confirmed by the comparison of EDX analysis of mayenite before and after the oxidation reaction (Fig. 4.7). Synthesized mayenite is characterized by the presence of Ca, Al and O in atomic ratios of 1 : 0.96 ± 0.17 : 3.1 ± 0.3, in line with the theoretical value for pure mayenite (Fig. 4.7a). After the oxidation reaction, Ca, Al and O are still detected (Fig 4.7b) but the signal of Cl can be pointed out. EDX analysis shows that Cl is uniformly distributed on mayenite sample (3.0 ± 1.1 % wt) and that there is a decrease of oxigen content. Ca, Al, O and Cl show atomic ratios of 1 : 0.95 ± 0.16 : 2.9 ± 0.3 : 0,10 ± 0.05, which are consistent with the formation of chloro-mayenite. The signal of C has not been taken into account in each spectra, because the samples have been placed on carbon disk and there is not statistically difference between C signal from the mayenite samples and from the substrate.

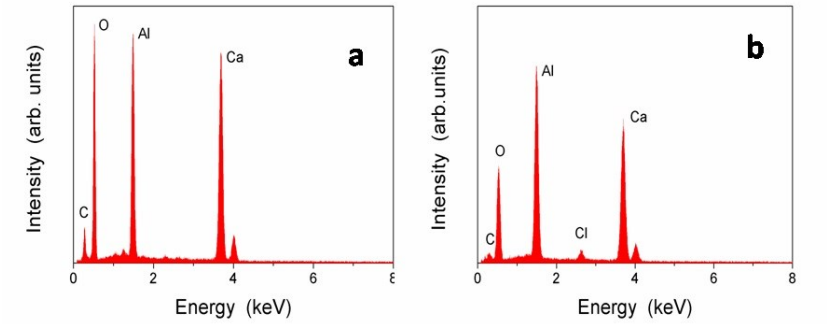

Figure 4.7 EDX spectra of mayenite a) before and b) after the oxidation reaction

Thus, the presence of Fe on the mayenite structure did not alter the selectivity of the reaction, and the main products observed are CO_2, CO and HCl (absorbed as chloro-mayenite).

Catalyst stability tests were also performed for 2.0% Fe/mayenite in comparison with pure mayenite, subjecting the catalyst sample operate for several hours (12 h) at operative conditions (T = 460°C, 1700 ppm TCE, GHSV = 6000 h^{-1}, 0.8 g of catalyst).

The results (Fig. 4.8) showed that the addition of iron in the mayenite framework, allowed to improve the stability of the material. Indeed, a partial deactivation (from 95% to 80% of TCE conversion) of 2.0 % Fe/mayenite was observed only after 12h, where pure mayenite is totally deactivated after 6h.

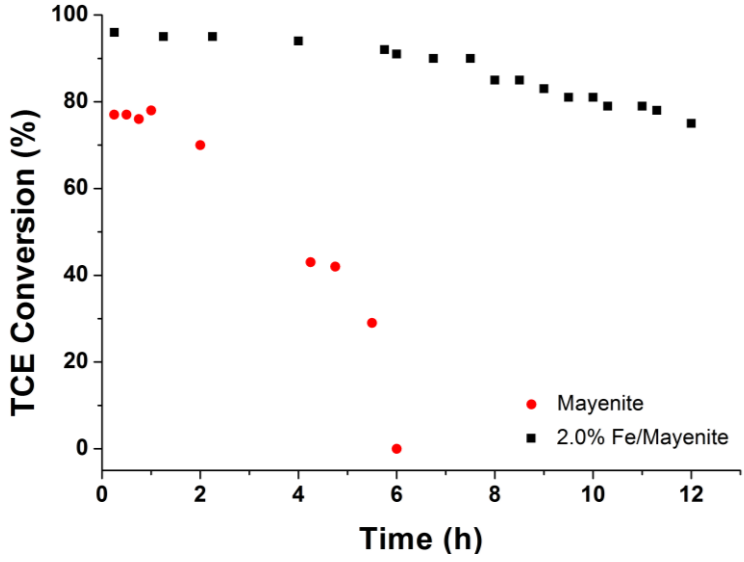

Figure 4.8 Comparison of catalysts stability (T=460°C, [TCE] 1700 ppm flux= 110 mL/min, GHSV = 6000 h^{-1}, 0.8 g of catalyst)

In order to clarify the deactivation mechanism of mayenite and 2% Fe/mayenite catalysts, XRD spectrum and SEM images of fresh and used catalyst were recorded.

XRD patterns of mayenite, before and after catalytic oxidation reaction, are reported in Figure 4.9. Results show only a crystalline structure change of the mayenite catalyst due to the reaction conditions (460°C).

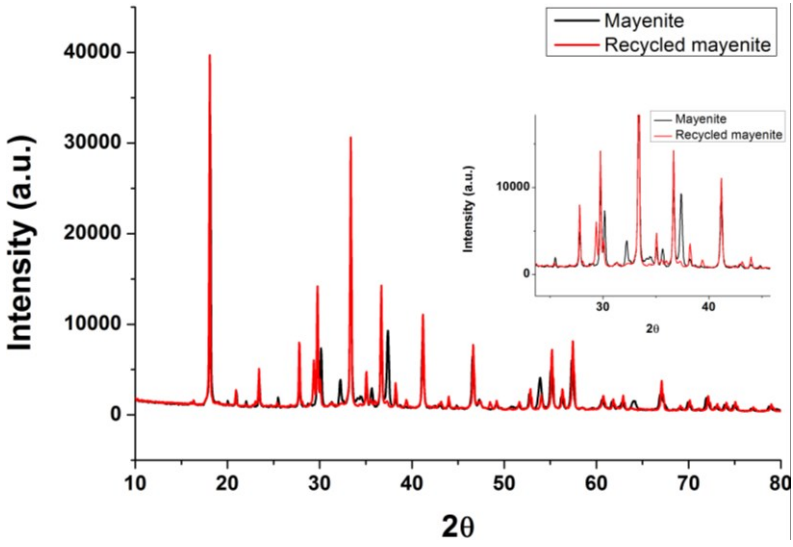

Figure 4.9 XRD patterns of mayenite before (black line) and after (red line) catalytic oxidation reaction. The inset shows a detail of the range 20 < 2θ < 45

Furthermore, the presence of a new peak related with chloride-mayenite (38.4°) could suggest a reaction of the HCl formed with the basic sites of the catalyst. This result confirmed that deactivation mechanism of mayenite catalyst is due to the displacing of the free oxygen species by chloride ions to form chloro-mayenite. Same XRD results (not showed) were obtained for 2.0 % Fe/mayenite at the end of the stability test, confirming the high thermal resistance of these materials.

In figure 4.10a and 4.10b SEM images of mayenite before and after the stability test are reported, respectively.

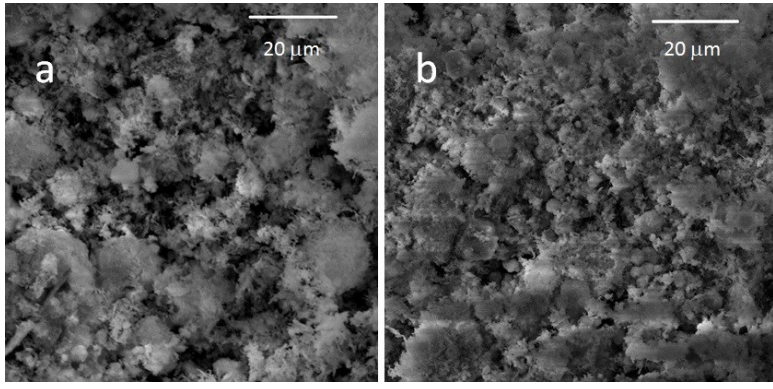

Figure 4.10 SEM images of mayenite a) before oxidation reaction and b) after oxidation reaction

Any significant morphological changes are detected before and after the oxidation reaction and mayenite is characterized by significant porosity which still remain (Figure 4.10b). In fact, the presence of sheets and two types of pores can be pointed out: large macropores on the µm scale and mesopores on the nm scale. SEM-EDX results of 2.0 % Fe/mayenite before and after the stability test are showed in figure 4.11.

As it can be seen, pure 2.0% Fe/mayenite is composed of calcium, aluminium, oxigen and minor amount of iron in the following wt% composition: 34 ± 3, 40 ± 5, 26 ± 3, and 1.9 ± 0.3, respectively (a).

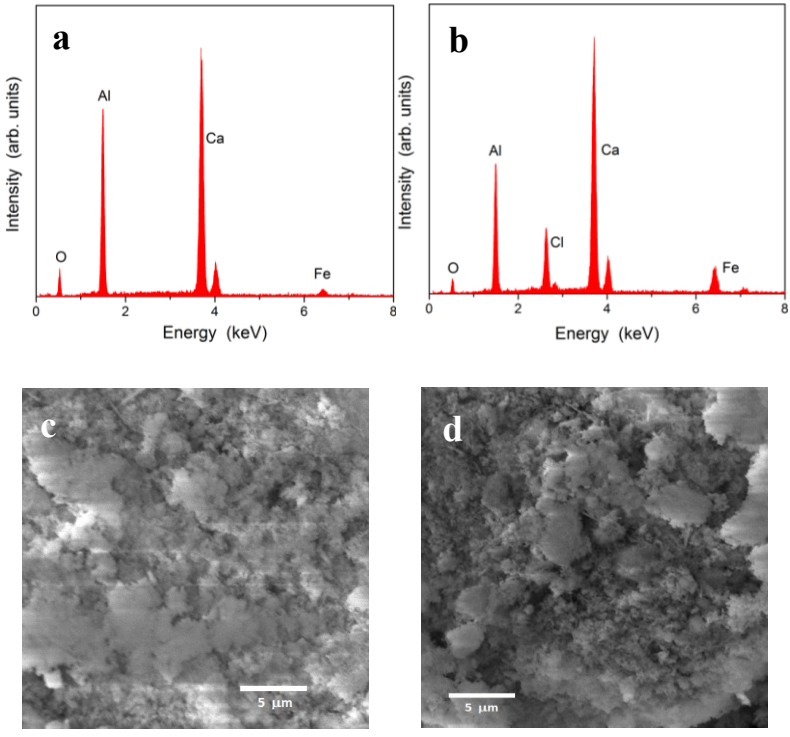

Figure 4.11 EDX spectra and SEM images of 2.0% Fe/mayenite before (a, c) and after (b, d) the stability test

Considering the uncertainty associated to the iron concentration, it can be said that it is uniformly distributed on mayenite. Moreover Fe/mayenite retains the same porosity observed for pure mayenite (c). In the same way of mayenite, Fe/mayenite continues to be a porous material with the presence of mesopores and macropores at the end of the stability test(d). Furthermore, the EDX analysis (b) shows the presence of an uniformly distributed chlorine, in 4.0 ± 0.9 wt%. Thus, deactivation mechanism of Fe/mayenite is due to

the chlorine poisoning, as observed for pure mayenite, and also probably by the formation of iron (III) chloride.

4.7.2 Influence of the preparation method on mayenite activity (Spain)

XRD spectra of the catalysts prepared with the 3 different routes are reported in fig. 4.12. Mayenite structure was indexed within I-43d group and showed the characteristic peaks of mayenite around 2θ = 18.1°, 30°, 33.4°, 36.7°, 41.2°, 46.7°, 55.2° and 57.4°. $Ca_3Al_2O_6$ (●) and $CaAl_2O_4$ (Δ) were also in this case found in trace as impurities formed during the mayenite synthesis[46].

As it can be seen, Maye HA presented broader and less intense peaks respect to the others mayenites, indicating a smaller crystallite size due to the less temperatures used for the calcination of the material.

Table 4.4 shows the BET surface area and the H_2-TPR results of the materials. Mayenite prepared by hydrothermal method showed higher BET surface area compared to the others synthesized catalysts.

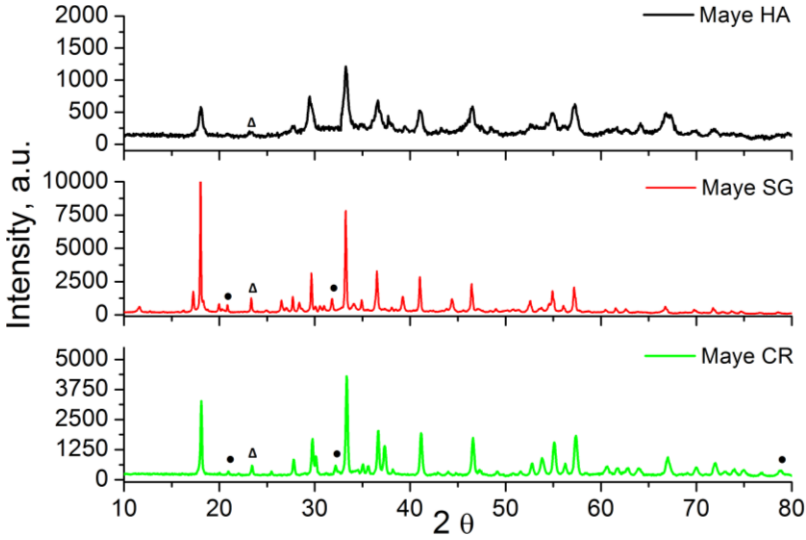

Figure 4.12 XRD spectra of prepared catalysts: Hydrothermal mayenite (black), Sol-gel Mayenite (red), Ceramic Mayenite (green)

This result is in line with XRD spectra reported above, where the high surface area of the material is related to its low crystallite size.

Table 4.4 BET surface area and TPR results for the different catalysts synthesized

Catalyst	**BET surface area (m^2/g)**	**H_2-uptake (mmol H_2/g)**
Maye HA	35.5	1.19
Maye SG	14.9	1.16
Maye CR	11.7	0.45

The hydrogen consumption in the TPR measurements was quantified by integrating the area under the reduction peaks

(fig. 4.13), and allowed to assess the oxidative properties of the mayenite catalysts.

As clearly shown by figure 4.13, Maye HA exhibited the same hydrogen consumption of Maye SG and they are much higher than that of Maye CR.

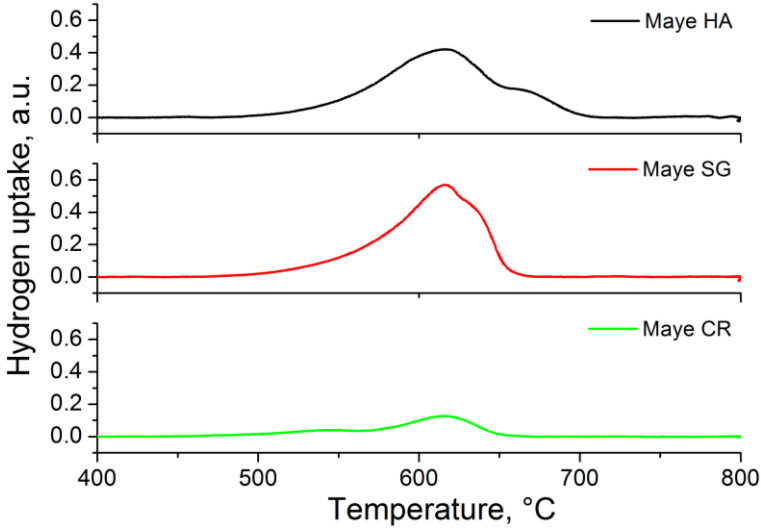

Figure 4.13 TPR profiles of mayenite HA, SG and CR

These results were in accordance with previous reported by Ruskaz et al., where they used TPR to estimate the fraction of extra-framework anions in mayenite that could be reduced[32]. In particular, Maye HA showed an higher population of O^{-x} and O_2^{-2} anions compared to Maye SG and CR. Moreover, nitrite and nitrate impurities in Maye SG are responsible of the hydrogen consumption comparable to that obtained using Maye HA[63].

The synthesized catalysts have been evaluated for the oxidation of trichloroethylene by monitoring the conversion as function of the temperature. Fig. 4.14 reported the light off curves for a blank experiment, Maye HA, SG and CR in absence of water. For blank experiments (thermal oxidation) there was no conversion below 500 °C, where in presence of maye HA, the catalytic activity started at around 200 °C.

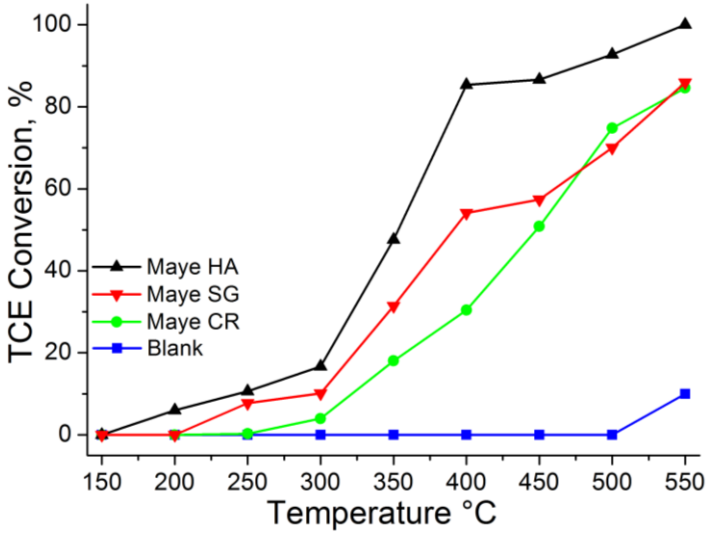

Figure 4.14 TCE conversion in a blank experiment (blue), with Maye HA (black), Maye SG (red) and Maye CR (green)

As clearly shown in Fig.4.14, mayenite prepared by the hydrothermal route showed better performance in absence of water than the other mayenites. The catalyst $T_{50\%}$ was around 350 °C, whilst for Maye SG and CR was respectively 390 °C and 450 °C. The conversion yield was found to increase

drastically with the temperature, until a total conversion was reached at 550 °C for Maye HA, where for Maye CR and SG only the ≈ 85% conversion of the pollutant was obtained.

The differences in the catalytic activity can be related with the different physico-chemical properties of the synthesized materials.

Mayenite prepared by hydrothermal route presented the highest surface area (35.5 m^2 g^{-1}), the highest hydrogen consumption (1.19 mmol H_2 g^{-1}) and the highest activity. This result confirmed our previous work (paragraph *4.7.1*) where we reported that the activity of the mayenite is related to the presence of $O^{2-}$and O_2^{2-} anions sites that favour the total oxidation of TCE[10,11]. It seems that mayenite synthesized by the hydrothermal method has a good combination of surface area and redox properties that explain the great activity of this material in the TCE oxidation reaction.

The effect of water vapour in the TCE oxidation was also investigated. The results showed that the addition of water to the feed stream did not alter the activity of the materials.

The selectivity of the reaction was also evaluated and the main oxidation products obtained in the trichloroethylene oxidation, were carbon dioxide (CO_2), carbon monoxide (CO) and hydrogen chloride (HCl). At all the investigated temperatures, chlorine (Cl_2) and tetrachloroethylene (PCE)

were only detected at low concentration.

Carbon selectivity (S_{CO} and S_{CO_2}) at 550 °C (T of maximum conversion) was calculated from equations (2) and (3) and reported in Table 4.5.

$$S_{CO} = \frac{CO}{(CO+CO_2)} \cdot 100 \quad (2)$$

$$S_{CO_2} = \frac{CO_2}{(CO+CO_2)} \cdot 100 \quad (3)$$

where CO and CO_2 are the concentration of carbon monoxide and dioxide in the outlet gases, expressed in ppm.

Table 4.5 Catalysts carbon selectivity at 550 °C

Catalyst	**S_{CO} (%)**	**SCO_2 (%)**
Maye HA	30	70
Maye SG	45	55
Mare CR	60	40

Maye HA showed an higher selectivity towards CO_2 than those of maye SG and maye CR; this result can be related with the best redox properties of maye HA that allow to favour the complete oxidation of TCE, especially at high temperatures (> 450 °C). Moreover, concerning the selectivity towards the chlorinated species, HCl was the main product observed for all the investigated catalysts, with Cl_2 detected only as traces. The HCl selectivity among the different

materials was calculated by using equation (4) and reported in Table 4.6.

$$S_{HCl} = \frac{HCl}{Cl_{inlet}} \cdot 100 \quad (4)$$

where HCl and Cl_{inlet} are the outlet gases concentration of hydrochloridric acid and the total Cl inlet concentration (≈ 3000 ppm) respectively.

Table 4.6 Catalysts HCl selectivity at 550 °C

Catalyst	**S_{HCl} (%)**
Maye HA	14
Maye SG	13
Maye CR	17

As clearly shown, the absence of a great amount of HCl was noted. This result confirmed our previous study, where the formation of chloro-mayenite, due to the replacing of free oxygen ions with chlorides, was recognized[31,41,53]. Furthermore, wet (1.7 %) experiments were also repeated and the results showed that no differences in term of product distribution between dry and wet conditions were observed.
Finally, catalyst stability was also evaluated for the best material (HA) synthesized, subjecting the mayenite catalyst operate for long on-stream periods at stationary conditions.

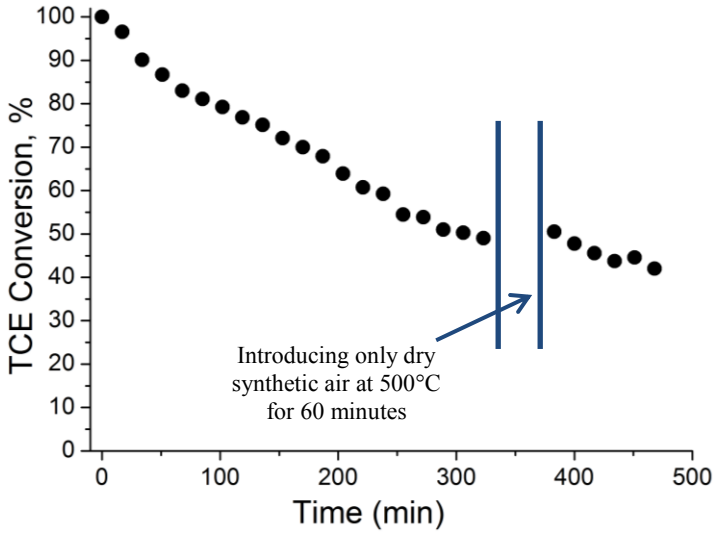

Figure 4.15 TCE conversion over mayenite HA at 500 °C for 475 min. (maye HA = 0.7 g, [TCE] = 1000 ppm, flux = 400 mL/min, GHSV =12000 h^{-1}, T = 500 °C)

As shown in Fig. 4.15, a moderate and progressive deactivation of Maye HA, with a decrease in the TCE conversion from 100 to 50 % after 325 min of time-on-stream was observed. In order to clarify the deactivation mechanism of the catalyst, FESEM images of maye HA were recorded before and after the stability test (Fig 4.16).

The results showed that only a limited morphological structure change due to the operative conditions was observed, confirming our previous study, where a great thermal stability of mayenite was noted (Fig.4.10)[31].

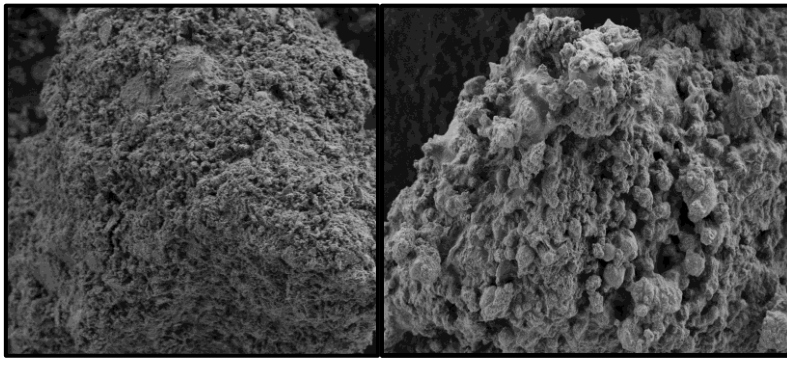

Figure 4.16 FESEM images of mayenite HA before (left) and after (right) stability test (2μm)

Figure 4.17 reported the XRD patterns of Maye HA, before and after the catalytic oxidation test.

As it can be seen, at the end of the reaction, no particular crystalline structure change of mayenite catalyst due to the reaction conditions were observed. However, the presence of a new peak (38.4°) related with chloride-mayenite, suggested a possible reaction of the in-situ formed HCl with the basic sites of the material, as described in the previous chapter[31,41,53].

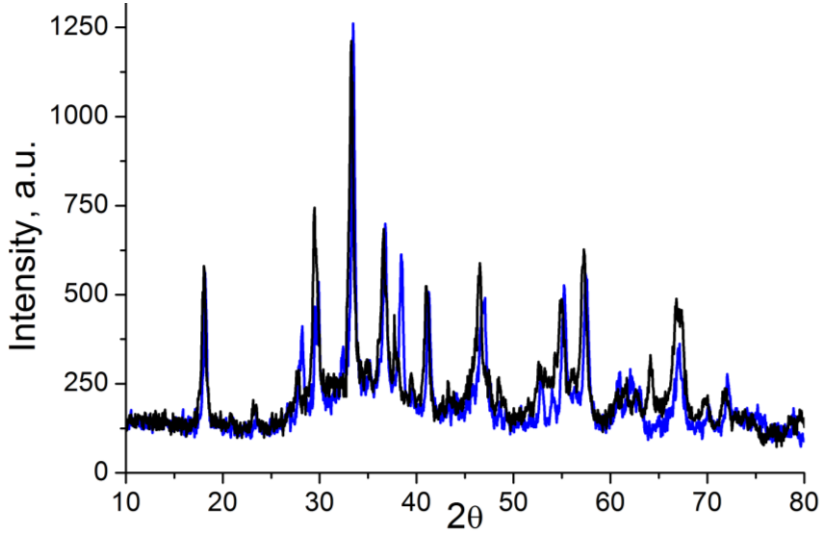

Figure 4.17 XRD patterns of mayenite before (black line) and after (blue line) the stability test

This result was validated by EDX analysis, as showed in Fig. 4.18 a and 4.18 b.

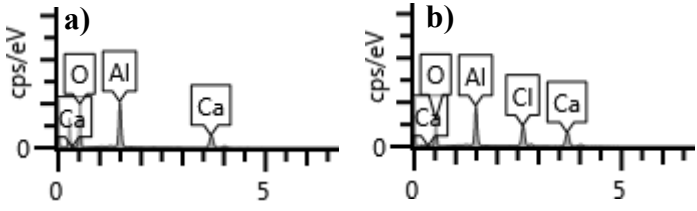

Figure 4.18 EDX spectrum of mayenite HA (a) before and (b) after the stability test

At the end of the reaction, Cl is uniformly distributed on mayenite HA sample and a decrease in the oxigen content respect to the starting material was observed, definitively

confirming our hypothesis about chloro-mayenite formation.
Based on this results, we studied the possibility for the ‘‘free oxygen’’ restore of the used material. Deactivated catalyst was flowed by dry synthetic air for 60 min at 500 °C, then reacted again at the same conditions. As clearly shown in Fig.4.15, deactivated catalyst was not restored, and chloro-mayenite was more stable than mayenite. This result is in line with those reported by Li et al., where it was shown that sulphide-mayenite was hardly restored by flowing O_2[49].
Catalyst stability for wet conditions (1.7%) was also checked and the results showed that the presence of water did not alter the deactivation process of the catalyst.

4.7.3 Improving mayenite features for the TCE oxidation using PMMA as a soft template agent (Spain)

In order to improve hydrothermal mayenite (in this paragraph namely mayenite) performances for the TCE oxidation, we developed a new synthetic procedure, based on the addition of different amount of PMMA as a soft template agent during mayenite synthesis.
XRD spectra of mayenite 10 (with the addition of 10% of PMMA in the synthesis), is reported in Figure 4.19. The synthesized catalyst showed the characteristic peaks of mayenite (Δ) (2θ = 18.1°, 30°, 33.4°, 36.7°, 41.2°, 46.7°,

55.2° and 57.4°); moreover calcite ($CaCO_3$, ●) impurities were also observed. The formation of the additional phase was due to the reaction from impurities of CaO unreacted and CO_2 produced by residual template combustion.

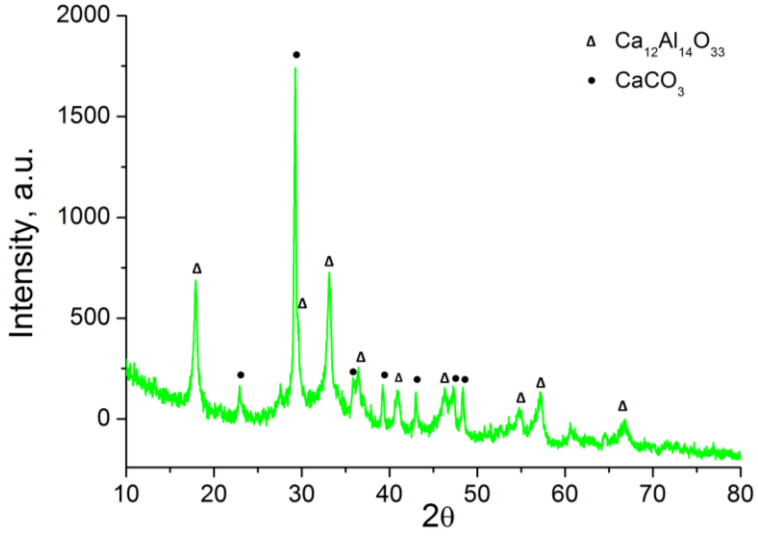

Figure 4.19 XRD spectrum of mayenite 10

Calcite impurities in mayenite 10 were quantified by TGA (Fig. 4.20) experiment and were found less than 10%[63]. Nevertheless, calcium carbonate is not involved in the TCE oxidation reaction.

The BET surface area of the synthesized catalysts are reported in table 4.7. As clearly shown, mayenite 10 showed the highest surface area. A further increase in the amount of

PMMA added in the synthesis (20%), did not allow an additional increase of the surface area of the material.

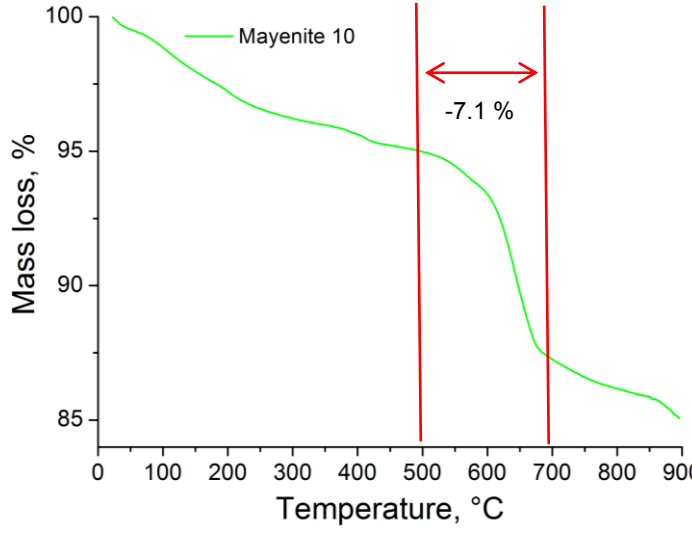

Figure 4.20 Thermogram of mayenite 10. $CaCO_3$ impurities decomposed (-7.1%) in T_{range}= 500-700 °C

Table 4.7 BET surface area of the synthetized catalysts

Catalyst	**BET surface area (m^2/g)**
Mayenite	35.5
Mayenite 10	47.1
Mayenite 20	41.9

Figure 4.21 shows the comparison of the Raman spectra among mayenite and mayenite 10. A peak at 1085 cm^{-1} confirmed the presence of the superoxide anions (O_2^-) in our materials[52].

As it can be seen mayenite 10 exhibited an higher concentration of oxygen active species respect to pure mayenite.

As described above, mayenite activity is related to the presence of O^{2-} and O_2^{2-} anions sites that could be favour the total oxidation of atmospheric pollutants[47,49,50]. It seems that the addition of PMMA in the catalyst synthesis allowed to increase the surface area and the number of free oxygens trapped in the mayenite structure, thus potentially enhancing catalytic performances.

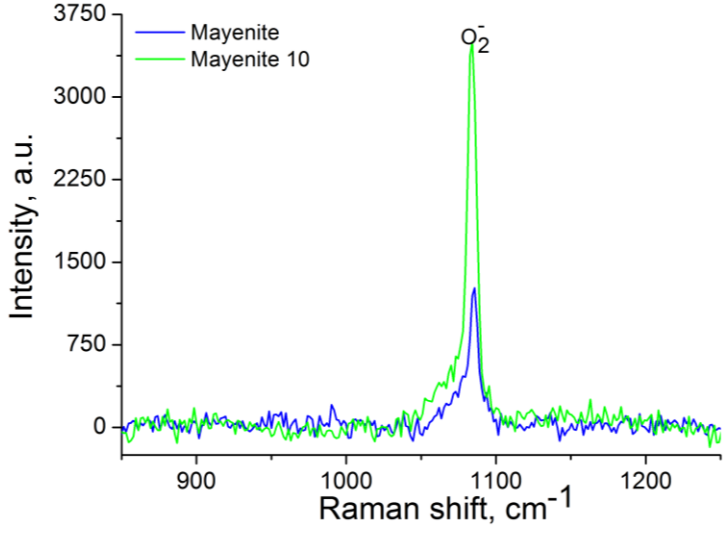

Figure 4.21 Raman spectra of mayenite (blue) and mayenite 10 (green) catalysts

The microstructure of the catalysts was also investigated and the FESEM images are reported in Fig 4.22. As it can be seen

the microstructure of the two materials was different, in particular mayenite 10 was characterized by two types of sheet, while for mayenite only one type was observed.

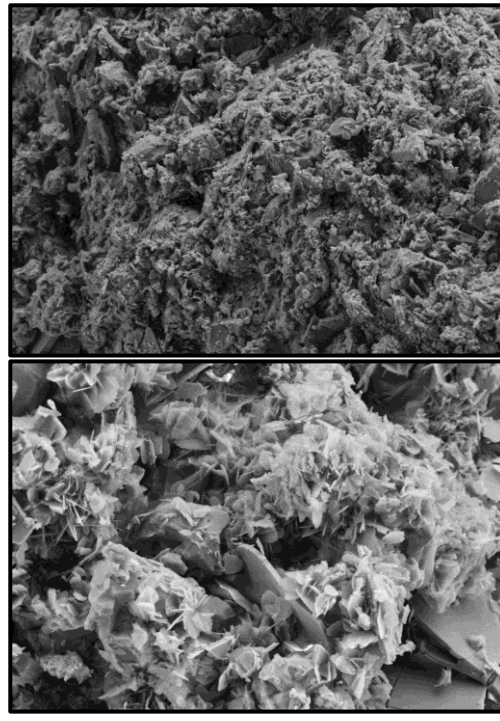

Figure 4.22 FESEM images of mayenite (top) and mayenite 10 (bottom) catalysts (1μm)

The light off curves of the synthesized mayenites for the TCE oxidation are reported in Fig.4.23.

As clearly shown, mayenite 10 was found the best catalyst in terms of T_{10} and T_{90}. At 200°C, it was able to degrade (8% of conversion) TCE, while mayenite and mayenite 20 were still inactive. The catalyst T_{50} and T_{90} for mayenite 10 were around

350 °C and 440°C, whilst for mayenite and mayenite 20 were 350/490°C and 370/450 °C, respectively.

As for the studies reported above, the differences among the catalytic activity of the three materials must be related to their different physico-chemical properties. In particular, the highest BET surface area (47.1 m^2/g) and the highest amount of O_2^- (active species in the total oxidation of TCE) represented the main features determining the best catalytic performances observed[31,55] for mayenite 10.

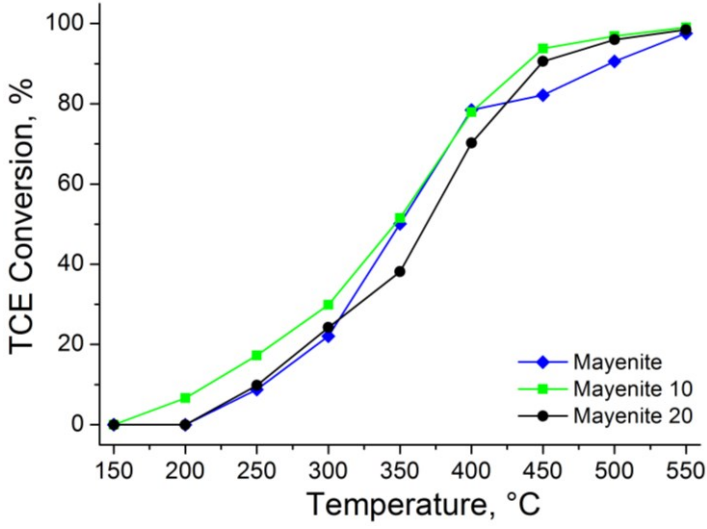

Figure 4.23 TCE conversion (1.7% H_2O) for mayenite (blue), mayenite 10 (green) and 20 (black)

Thus, in order to prepare an active catalyst for the TCE oxidation, an optimum combination of high surface area and oxidative properties is required. Those can be obtained

preparing mayenite based-catalyst by adding PMMA as soft template agent.

Reaction selectivity was also evaluated and the results showed that the main TCE oxidation products were CO_2, CO and HCl, confirming our studies described above[31,53-55].

Catalyst stability was evaluated for the best material synthesized (mayenite 10), subjecting the catalyst operate for several hours at operative conditions (0.7g, 1000 ppm TCE, 400 mL/min, 12.000 h^{-1}, 1.7% H_2O, 500°C).

Figure 4.24 reports the comparison of catalyst stability curve for mayenite 10 and pure mayenite used as reference material.

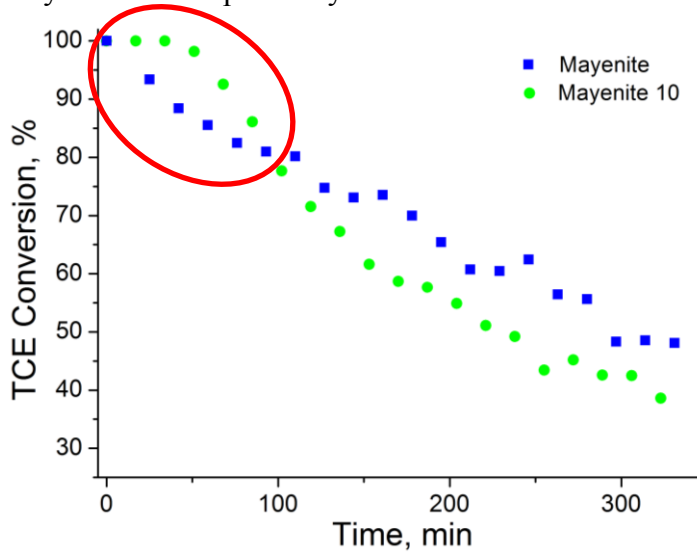

Figure 4.24 Stability test for mayenite (blue square) and mayenite 10 (green circle) catalysts, (0.7g, 1000 ppm TCE, 400 mL/min, 12000 h-1, 1.7% H_2O, 500 °C)

As highlighted by the red circle, for the first 2h, mayenite 10 was found more active and stable than mayenite. After, a rapid deactivation occurred and mayenite 10 was found less active than mayenite. XRD patterns of used mayenite 10 (Fig. 4.25) allowed to clarify the deactivation mechanism of the catalyst.

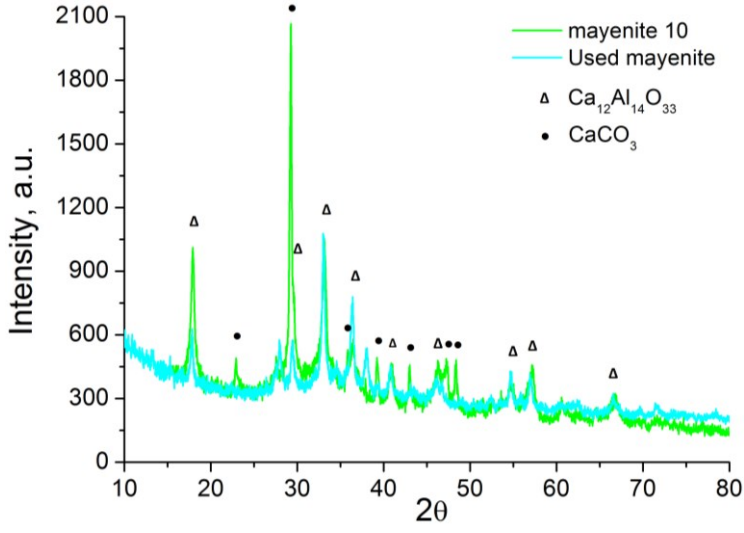

Figure 4.25 XRD patterns of mayenite 10 before (red line) and after (green line) stability test (0.7g, 1000 ppm TCE, 400 mL/min, 12000 h^{-1}, 1.7% H_2O, 500 °C)

The results showed that calcium carbonate impurities are responsible of the initial enhancement of mayenite 10 stability, thanks to the reaction between $CaCO_3$ and in-situ produced HCl (TCE oxidation product). XRD spectrum of used catalyst showed the disappearance of $CaCO_3$ phase at the end of reaction, confirmed so our deactivation hypothesis.

After, thanks to its great activity, mayenite 10 exhibited a very rapid deactivation compared to hydrothermal mayenite with the formation of chloro-mayenite, as already reported above[31,53-55].

4.8 Conclusion

In this thesis, we studied for first time the catalytic activity for the TCE oxidation of mayenite catalyst, prepared by ceramic synthesis. Moreover we prepared and tested Fe/mayenite with different metal loading. The results showed that mayenite was an active catalyst for the TCE oxidation, with 2.0% Fe/mayenite was the best catalyst prepared. TCE was totally converted in CO_2, CO and the released HCl was incorporated in the mayenite structure thanks to the replacing of the free oxygen ions with chlorides to form chloro-mayenite (Brearleyite $Ca_{12}Al_{14}O_{32}Cl_2$). The high performances of the material is related to its oxidative properties due to the presence of O^{2-} and O_2^{2-} anions sites that favour the total oxidation of TCE and avoid the formation of coke. In case of Fe/mayenite, the improved performance are correlated with an optimum combination of the oxidative properties of mayenite (free oxygen species) and the great catalytic activity of the metal.

After that, thanks to an Erasmus traineeship project, I continued this research at the ITQ-UPV (Spain). Here we evaluated the influence of the preparation method (ceramic, sol-gel and hydrothermal) on the mayenite activity for the TCE oxidation.

All the synthesized catalyst were active in the TCE oxidation reaction, where mayenite prepared by hydrothermal route showed the best performance, due to an optimum combination of surface area and redox properties that explain the enhanced activity of this material. The effect of water vapour on the TCE catalytic oxidation was also investigated and the results showed that the addition of water to the gas stream did not alter the activity, the selectivity and the stability of all the catalysts investigated.

In the last part of this project we used PMMA to improve mayenite performances in the TCE oxidation reaction.

Mayenite prepared adding 10% w/w of PMMA, showed better performances respect to all previous mayenite synthesized.

The high performances of mayenite is related to an optimum balance of high surface area and large number of superoxide anions that favour the total oxidation of the pollutant at lower temperature.

As conclusion we can state that in order to obtain an active catalyst for the TCE oxidation, we need a good combination

of oxidative properties and high surface area; In this direction mayenite catalyst could be a good candidate for this type of reaction.

Moreover, respect to previous catalytic systems, mayenite presented several distinctive advantages, namely *i*) a total conversion of TCE in less harmful Cl^- and CO_2, *ii*) the presence of free O^{2-} ions made unnecessary the use of noble and heavy metals, thus reducing the costs and the environmental impact at the end of the material life-cycle and *iii*) inexpensive precursors for the material synthesis, such as calcium and aluminium hydroxides.

References

(1) Heck R.M. et al., Wiley-Interscience, New York, **2002**
(2) Scirè S. et al., *Appl. Catal. B: Environ.* **2012**,125, 222-246
(3) Amann M. et al., M. Lutz, *J. Hazard. Mater.* **2000**, 78,41-62
(4) Rossi F. et al., *Aiche J.*, **2015**,61,3511-3515
(5) Aranzabal A. et al., *Chem. Pap.* **2014**,68,1169–1186
(6) Tomatis M. et al, *Journal of Chemistry.* **2016**, Article ID 8324826
(7) Kamal M.S. et al., *Atmos. Environ.* **2016**,140,117-134
(8) Moretti E.C., *Chem. Eng. Prog.* **2002**,98,30-40
(9) Liotta L.F., *Appl. Catal. B: Environ.* **2010**,100,403-412
(10) Pitkäaho S. et al., *Appl. Catal. B: Environ.* **2011**,102, 395–403
(11) Joung H.J. et al., *Appl. Surf. Sci.* **2014**,290, 267-273
(12) Lopez-Fonseca R. et al., *Catal. Today.* **2005**,107–108, 200-207
(13) Wang Y. et al, *Catal. Today.* **2015**,242,294-299
(14) Han W. et al., *Ind. Eng. Chem. Res.* **2014**,53,3486-3494
(15) Ali A.M. et al., *Appl. Catal. A: Gen.* **2015**,489, 24-31
(16) de Rivas B. et al., *WIT Trans. Ecol. Environ.* **2008**,109,857–866
(17) de Rivas B. et al., *Chem. Eng. J.* **2012**,184, 184-192
(18) Assebban M., *Chem. Eng. J.* **2015** 262,1252-1259
(19) Blanch-Raga N. et al., *Appl. Catal.B: Environ.* **2016**,187,90–97
(20) Li S., et al. *Appl. Catal.B: Environ.* **2015**,166-167, 260-269
(21) Blanch-Raga N. et al., *Appl. Catal.B: Environ.* **2013**,130-131,36-43
(22) Wang J. et al, *Catal. Commun.* **2016**, 76,13-18
(23) Cui J.X. et al., *Chem. Eng. J.* **2017**,313,815-825
(24) Blanch-Raga N. et al., *Ind. Eng. Chem. Res.* **2013**,52,15772−15779
(25) Romero-Sáez M. et al, *Appl. Catal.B: Environ.* **2016**,180,210–218
(26) Dinh, M.T.N. et al., *Appl. Catal.B: Environ.* **2015**,172,65-72
(27) López-Fonseca R. et al., *Appl. Catal. A Gen.* **2004**,271,39–46
(28) Blanch-Raga N. et al., *Appl. Catal.B: Environ.* **2014**,160,129-134
(29) Aranzabal A. et al., *J. Catal.* **2012**,296,165-174
(30) Divakar D. et al., *Catal. Today.* **2011**, 176,357–360
(31) Cucciniello R. et al, *Appl. Catal. B: Environ.* **2017**,204,167-172
(32) Ruszak M. et al., *Res. Chem. Intermed.* **2007**,33,689–703
(33) Dong Y. et al., *RSC Adv.* **2013**,3,18311-18316
(34) Hayashi K. et al., *J. Phys. Chem. B.* **2005**,109,11900-11906
(35) Hayashi K. et al., *J. Phys. Chem. B.* **2007**,111,1946-1956
(36) Hayashi K. et al., *J. Am. Chem. Soc.* **2002**,124,738-739
(37) Hayashi K. et al., *Nature.* **2002**, 419, 462-465
(38) Kitano M. et al., *Nat. Chem.* **2012**,4,934–940
(39) Hayashi F. et al., *J. Am.Chem. Soc.* **2014**,136,11698-11706
(40) Proto A. et al., *Catal. Commun.* **2015**,68,41-45

(41) Schmidt A., *Solid State Ion.* **2014**,254,48–58
(42) Eufinger J.P. et al., *Phys. Chem. Chem. Phys.* **2015**,17,6844–6857
(43) Maurelli S. et al., *Phys. Chem. Chem. Phys.* **2010**,12,10933–10941
(44) Huang J. et al., *Chem. Mat.* **2015**,27,4731−4741
(45) Vernoux P. et al., *Chem. Rev.* **2013**,113,8192-8260
(46) Lacerda M. et al., *Nature.* **1988**,332,525–526
(47) Teusner M. et al., *J. Phys. Chem. C*. **2015**,119,9721–9727
(48) Teusner M. et al., *Solid State Ion.* **2016**,284,25–27
(49) Li C. et al., *App. Cat. B: Environ*. **2009**,88,351-360
(50) Yang S. et al., *Appl. Cat. A: Gen*. **2004**,277,239-246
(51) Ruszak M. et al., *Cat. Lett.* **2008**,126,72-77
(52) Fujita S. et al., *Catal. Lett.* **2006**,106,139-143
(53) Intiso A. et al., *Advances in Bionanomaterials* **2017**,131-139
(54) Intiso A. et al., *J. Haz. Mat.* submitted **2017**
(55) Intiso A. et al., *App. Cat. B. Environ.* submitted **2017**
(56) Solsona B. et al., *Catalysts.* **2017**,7, 96
(57) Intiso A. et al., *Cat. Comm*., in preparation
(58) Li C. et al., *Mat. Res. Bull*. **2011**,46,1307–1310
(59) Molina R. et al., *J. Catal.* **1998**,173,257-267
(60) Ude S.N. et al., *Ceram. Int.* **2014**,40,1117–1123
(61) Proto A. et al., *Environ. Sci. Poll. Res.* **2013**,21,3182–3186
(62) Mendez M. Et al., *Atmos. Chem. Phys.* **2013**,13,11661–11673
(63) Cucciniello R. et al., *Atmos. Environ.* **2013**,79,666–671

Conclusions

TCE is one of the most detected pollutants, present in all the compartments of the environment. During the period of PhD activity we attempted to build a multidisciplinary approach to solve the problem of TCE polluted sites. In particular, three remediation strategies (surfactant co-solvent flushing, phytoremediation and catalytic oxidation) were investigated with the intention to improve the technology in terms of environmental sustainability, and costs.

First of all, we characterized the diffusion mechanism of TCE in water, to improve the models used to describe the fate of the pollutant in the groundwater before and during the remediation strategy. In particular, we have presented a method based on the Taylor Dispersion Analysis (TDA), which allowed to measure for the first time the diffusion coefficient of TCE in water. The results showed that at 25°C $D_{TCE} = 8.16 \pm 0.06 \times 10^{-6}$ cm^2 s^{-1} and the value increases almost linearly with the temperature. The obtained results are fundamental to improve the advection-dispersion models used to predict the fate of TCE in the environment.

After, we focused our attention on two remediation techniques usually employed for the removal of TCE from contaminated sites. First, with the aim to improve surfactant co-solvent flushing technologies for groundwater remediation, we

investigated the capability of Synperonic 91/5 (Syn 91/5) to enhance the aqueous solubility of TCE.

Syn 91/5 was selected thanks to its features, in particular it is a commercially available and cost effective synthetic ethoxylated alcohol, known to be a low-impact and biodegradable "green" surfactant. The results showed that the maximum solubility found at 20 °C (19.71 g/L in [SYN] = 1 M) was almost 15 times greater than the solubility in pure water (1.280 g/L). Moreover, the dependence of the solubilized TCE with respect to the concentration of the surfactant was found to be linear in the interval 0.1–0.7 M. Finally, the influence of the temperature on the TCE solubility was also evaluated, showing for the lowest value (4°C) the highest solubility (26.3 g/L in [SYN] = 1 M).

Subsequently, we investigated phytoremediation as a green alternative for the clean-up of TCE polluted sites. In particular we tested the phytoremediation capability of *zea mays* (also known as corn plant) to metabolize TCE from an artificial polluted medium. Corn plant presents some advantages (wide fasciculate root apparatus, great biomass production etc.) with respect to many other plant species previously used for phytoremediation studies. The results showed that after 9 days of exposition, plant adsorbs and degrades TCE with an efficiency ranging from 15 to 20 % of the initial TCE present

in the system. Moreover plant extracts revealed the presence of several TCE metabolites, suggesting that *Z. mays* followed the Sandermann green liver metabolic model.

The last part of this PhD project was focused on the development of new green catalysts for the total oxidation of TCE. In this context we successfully demonstrated that mayenite ($Ca_{12}Al_{14}O_{33}$) is an active material for the complete oxidation of TCE. This result is due to the presence of O^{2-} and O_2^{2-} anions in the micro-cages of the mayenite, which favoured the total oxidation of TCE and avoided the formation of coke.

After we evaluated how transition metals such as iron, could improve mayenite activity. The results showed that the presence of only 2% of Fe on mayenite (as Fe_2O_3) surface, allowed to improve catalyst activity, reducing the operative temperature for the total oxidation of TCE in the range of 250-450 °C.

The last six months of this project were spent in the ITQ-UPV, where we continued our research in this field. In particular, we evaluated the influence of different synthetic method on mayenite performances for the TCE oxidation reaction. Catalyst was synthesized by following different routes namely ceramic, sol-gel and hydrothermal. Mayenite prepared by the hydrothermal route showed the best

performances in terms of total conversion yield at the lowest temperature (T_{50}=350°C, T_{90}= 490 °C) and in terms of selectivity (CO_2, CO and HCl).

It seems that mayenite synthetized by the hydrothermal method has a good combination of surface area and redox properties that explain the great activity of this material in the TCE oxidation reaction.

The last part of this project was focused on the improvement of mayenite activity in the TCE oxidation reaction using PMMA as a soft template agent. Mayenite prepared adding 10% w/w of PMMA, was found the most active material respect to all previous mayenite synthesized. The high performance of mayenite is due to an optimum balance of high surface area and large number of superoxide anions that favour the complete oxidation of TCE at lower temperature.

In conclusion, in this PhD project we have demonstrated that a multidisciplinary approach is fundamental to solve the problem of DNAPLs polluted sites. During these three years, through the strong interaction with other groups, in particular with the CIMAV and the ITQ-UPV, we have obtained promising results that encouraging further investigations for in-field applications of green remediation technologies.